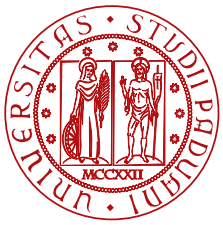

UNIVERSITÀ DEGLI STUDI DI PADOVA

DIPARTIMENTO DI INGEGNERIA DELL'INFORMAZIONE

DEPARTMENT OF INFORMATION ENGINEERING

MASTER COURSE IN

Bioengineering for the Neuroscience

Error-Related Potential identification during continuous control of a powered wheelchair

Supervisor
Prof. Luca Tonin

Author
Lorenzo Bergamini

ACADEMIC YEAR 2022-2023

Graduation date 14/12/2023

Abstract

Brain-Computer Interfaces (BCIs) represent groundbreaking technology, offering substantial improvements in the quality of life for individuals with severe motor disabilities. This study focuses on the identification of Error-Related Potentials (ErrPs) and their key characteristics during the continuous control of a powered wheelchair. Participants were instructed to navigate the powered wheelchair using a joystick along a predetermined path with obstacles, while EEG data were collected. ErrP was successfully identified when the wheelchair executed an unexpected command not initiated by the user. The analysis, including artifact removal and alignment of ErrP peaks, was performed offline. The obtained results are comparable to studies in the literature for discrete control. This groundbreaking finding holds significant implications for future advancements in continuous BCI control, aiming to enhance the user experience.

Sommario

Le Brain-Computer Interfaces (BCI) rappresentano una tecnologia rivoluzionaria, offrendo miglioramenti sostanziali nella qualità della vita per individui con gravi disabilità motorie. Questo studio si concentra sull'identificazione dei Potenziali di Errore (ErrP) e delle loro caratteristiche chiave durante il controllo continuo di una sedia a rotelle motorizzata. Ai partecipanti è stato chiesto di guidare la sedia a rotelle motorizzata utilizzando un joystick lungo un percorso prestabilito con ostacoli, mentre venivano registrati dati EEG. Gli ErrP sono stati identificati con successo quando la sedia a rotelle ha eseguito un comando inaspettato non generato dall'utente. L'analisi, comprensiva della rimozione degli artefatti e dell'allineamento dei picchi ErrP, è stata eseguita offline. I risultati ottenuti sono confrontabili con gli studi presenti in letteratura per il controllo discreto. Questa scoperta rivoluzionaria ha significative implicazioni per futuri progressi nel controllo continuo BCI, con l'obiettivo di migliorare l'esperienza dell'utente.

Contents

0.1 List of Acronyms

ACC Anterior Cingulate Cortex

AEP Auditory Evoked Potential

AMICA Adaptive Mixture of Independent Component Analysis

ANOVA Analysis of Variance

BCI Brain-Computer Interface

BMI Brain-Machine Interface

CAR common average reference

ECoG electrocorticography

EEG electroencephalography

EOG electrooculogram

EP Evoked Potential

ERN Error-Related Negativity

ERP Event-Related Potential

ErrP Error-Related Potential

fMRI functional magnetic resonance imaging

fNIRS functional near-infrared spectroscopy

MI Motor Imagery

PET Positron Emission Tomography

ROS Robot Operating System

SCP Slow Cortical Potential

SEP Somatosensory Evoked Potential

SMR Sensorimotor Rhythm

SSVEP steady-state visual evoked potential

VEP Visual Evoked Potential

Chapter 1

Introduction

In the current technological context, Brain-Computer Interfaces (BCIs), or Brain-Machine Interfaces (BMIs), play a prominent role in the development of medical devices [1] for individuals who have suffered severe damage to the nervous system due to various diseases such as stroke [2], acute inflammatory demyelinating polyneuropathy [3], and multiple sclerosis [4]. The challenge for these individuals is the inability to perform even the simplest daily tasks due to physical limitations, despite being cognitively active, and the inability to utilize assistive systems based on alternative pathways (such as eye gaze, mouth opening, tongue protrusion) to communicate the intention of movement [5]. BCIs serve as a bridge between the human and the computer to perform a specific activity. Through the acquisition of the brain signals, human intention is interpreted by the computer, translated into the required action, and executed by external devices. Wolpaw proposed the first definition of BCI: "Brain-computer interfaces give their user communication and control channels that do not depend on the brain's normal output channels of peripheral nerves and muscles." [Wolpaw et al., IEEE Transactions on Rehabilitation Engineering, 2000] [6]. To better understand the functioning of this technology, it is important to briefly describe the characteristics, functioning, and types of the different elements at play.

1.1 The Brain: a brief description

The brain can be divided into three main parts: the cerebellum, the brainstem, and the cerebrum, each with distinct functions [7]. The cerebellum plays a crucial role in motor control, coordination, sensory perception, and fine motor skills [8]. It contributes to regulating posture and balance and is involved in voluntary muscle movements. The brainstem serves as a vital bridge between the cerebellum and the spinal cord [9]. It is the central control panel of the body and oversees essential functions such as breathing, consciousness, eye and mouth movements, and the transmission of sensory messages, including pain, temperature, and sound [9]. It also

regulates vital processes such as heart rate, blood pressure, and hunger [10]. Finally, the most important and of greater interest to BCI is the cerebrum, responsible for a wide range of cognitive functions, including thoughts, movements, and emotions [8]. It is composed of neural tissues called the cerebral cortex and is divided into the left and right hemispheres, each further subdivided into four lobes [11]:

- The frontal lobe is associated with personality, emotions, problem-solving, motor development, reasoning, planning, language production, and voluntary muscle movements [12]
- The parietal lobe is responsible for sensations, sensory understanding, stimulus recognition, spatial orientation, and movement [8]
- The occipital lobe is primarily responsible for the visual process [11]
- The temporal lobe handles the recognition of auditory stimuli, language processing, perception, and memory [7].

Of particular interest is the area of the cingulate cortex. It is located in the medial part of the brain, above the corpus callosum and below the striatum, and is part of the limbic system [13]. For this reason, it is involved, along with structures contained within it, such as the amygdala, hippocampus, and cingulate gyrus, in multiple cognitive and emotional functions [14]. It is then divided into four different functional regions: anterior, medial, posterior, and retrosplenial [15]. The Anterior Cingulate Cortex (ACC) is the anatomical area of primary interest of this thesis since it is responsible for error detection and processing [16].

1.2 Acquisition Method

To record brain activity, various types of equipment have been developed and employed. The choice of instrumentation varies based on the ultimate goal since each technique has different characteristics. The most common ones include Positron Emission Tomography (PET), electrocorticography (ECoG) [17], functional near-infrared spectroscopy (fNIRS) [18], functional magnetic resonance imaging (fMRI) and electroencephalography (EEG) [17]. Currently, the only data acquisition techniques utilized by BCI technologies are ECoG and EEG.

1.2.1 Electrocorticography

ECoG represents an advanced neurophysiological technique that allows the recording of cortical potentials directly from brain tissue through the attachment or implantation of electrodes, making it classified as an invasive investigative method [19]. This method distinguishes itself from

EEG as it eliminates signal dispersion and attenuation caused by the presence of the scalp and skull [20], factors that can significantly compromise the amplitude of detected potentials [19]. The absence of these intervening structures allows ECoG to provide a more faithful and detailed representation of brain activity due to its high spatial and temporal resolution [20], making it particularly useful in operational contexts [21]. During surgical interventions where the brain is exposed, ECoG is employed to continuously monitor changes in cortical electrical activity [22]. This real-time monitoring capability is crucial during brain stimulations, enabling surgeons to assess the effect of stimulations directly on the cerebral cortex and evaluate activation areas [23]. A crucial aspect of the ECoG application is its ability to detect non-convulsive epileptiform activity [23]. This form of epileptic activity can manifest without apparent physical signs of seizures and may occur after electrical stimulation of cortical area [24].

1.2.2 Electroencephalography

EEG is a non-invasive technique for directly measuring brain electrical activity [25]. It is widely used in both clinical and research fields and is also employed in psychology and cognitive sciences to directly measure neuronal activity [26]. EEG has much better temporal resolution compared to other possible non-invasive systems like fMRI, PET, or fNIRS [27].

What is measured is a macroscopic phenomenon that reflects the synchronized activity of an extended neuronal population [25]. EEG primarily reflects the activity of cortical neurons as it is more challenging to measure deeper neurons within the brain due to the low signal power generated by these cells [28]. The neurons influencing measurements are pyramidal neurons, organized in parallel with each other and having a dendrite, called the apical dendrite, orthogonal to the brain's surface [29]. There are also other neurons that are not organized within the cortical surface with a predominant direction, and therefore, they do not overly influence the measured electrical activity due to their stochastic contribution [30].

What is measured with EEG is the postsynaptic potential [29]. The overall process leading to the measured signal can be described as follows: from a given neuron, an action potential is generated that will reach the target neuron, where a postsynaptic stimulus will be generated, i.e., the signal causing extracellular depolarization or hyperpolarization, depending on the type of synapse, which will be measured and detected in EEG signals [28]. Of course, the measured signal does not come from a single neuron but from a large number of neurons firing synchronously [29].

To measure the activity of pyramidal neurons, these types of cells must exhibit high temporal synchronicity and spatial summation that allows for generating a field potential strong enough to be measured from the scalp [31]. These neuronal activities generate currents that flow in the volume conductor of the head [32]. These are reflected as potential differences on the scalp

surface.
Key parameters of EEG include frequency, quantifying the number of waves per second expressed in Hertz (Hz), and amplitude, measured in microvolts (μV), of potential oscillations, known as EEG rhythms. Variations in these parameters reflect physiological events such as normal brain activity, concentration, sleep [33], and sensory stimulation [34]. Similarly, they can indicate pathological conditions such as tumors, hematomas, or epilepsy [35].

These rhythms are categorized based on the dominant frequency content, and the four main categories are:

- α rhythm: typically manifesting in frequencies from 8 to 13 Hz and often associated with relaxation or eye closure [36].
- β rhythm: having frequencies in the range [13-30] Hz, generally correlated with focused mental activity and excitement. They can be recorded in the frontal part of the head [37].
- γ rhythm: fluctuations with a relatively high frequency (30-80 Hz). It is influenced by sensory inputs and internal processes, such as attention and working memory [38].
- δ rhythm: referring to low frequencies (0.5-4 Hz), often present during deep sleep [39].
- ϑ rhythm: frequencies between 4 and 8 Hz, observable during sleep and in children up to 13 years old. If observed in awake adults, they may signal a subcortical lesion [40].

1.3 Electrophysiology

Electroencephalography can measure various types of signals; however, for the purpose of this study, only a few of these numerous signals will be briefly described: Evoked Potentials (EPs) and Event-Related Potentials (ERPs).

1.3.1 Evoked Potentials

EPs are electric responses of the central nervous system to external sensory or motor stimuli [41]. These can be generated by visual, auditory, or tactile stimuli and provide a means to study the speed and integrity of neural pathways involved in sensory perception and motor responses [42]. EPs are characterized and classified based on their waveform, specifically positive and negative peaks, and the temporal interval between the stimulus and the recorded fluctuation [43]. The uniqueness of these signals lies in being time-locked and stimulus-specific, presenting consistently in the same form and after the same time interval for each stimulus type [42]. However, the amplitude varies from subject to subject, and a decrease is observed when the

same stimulus is repeatedly presented to the same subject during an experiment [41]. Examples of evoked potentials include:

- Visual Evoked Potentials (VEPs): Recorded in response to visual stimuli, such as light flashes. VEP analysis can provide information about the functionality of optic pathways and visual processing in the brain [44].
- Auditory Evoked Potentials (AEPs): Recorded in response to auditory stimuli, such as sounds or tones. They can be used to assess hearing function and the integrity of auditory pathways [45]
- Somatosensory Evoked Potentials (SEPs): Measured in response to tactile stimuli. These can be used to assess the function of peripheral nerves and sensory pathways [45].

1.3.2 Event-Related Potentials

ERPs are a subset of evoked potentials representing variations in brain activity correlated with specific cognitive events [46]. While EPs depend on the physical characteristics of the stimulus, ERPs are related to the informational content of the stimulus and the meaning the subject attributes to it [47]. They are often used to study cognitive processes such as attention, memory, and perception [48]. Examples of ERPs include:

- P300: A positive potential (greater than 10 μV) associated with memory and attention processing, appearing only after 300 ms (hence the name P300) following "target" stimuli [49]. It has a characteristic distribution on posterior derivations (centro-parietal-occipital) [50]. For example, P300 can be recorded when an individual recognizes an unexpected or rare stimulus in a sequence of common stimuli.
- N400: Associated with language and semantic understanding. It is often recorded in response to sentences or words that violate semantic expectations [46].

Additionally, there are other brain rhythms not generated by external factors, but spontaneously modulated by individuals [51]. Examples include Sensorimotor Rhythms (SMRs) and Slow Cortical Potentials (SCPs):

- Sensorimotor Rhythms: Comprising alpha rhythms, also called mu rhythms, and beta rhythms [52]. The amplitude of these signals varies when brain activity is linked to motor tasks, even if actual movement is not required to modulate the intensity of these rhythms [53].

- Slow Cortical Potentials: Representing slow-duration voltage changes in EEG, extending from one to several seconds and connected to changes in cortical activity levels [54]. Negative SCPs are associated with increased neuronal activity, while positive SCPs occur simultaneously with decreased activity in individual cells [54].

1.3.3 Error Related Potentials

Error-Related Potentials (ErrPs) are a specific category of ERP reflecting neural processing related to the recognition and correction of errors in cognitive or motor tasks [55]. They are generated by the ACC and can be recorded from electrodes Fz, FCz, Cz, and Pz at the sagittal suture of the skull [56]. Like all other evoked potentials, ErrPs are time-locked to the beginning of the stimulus [57]. Four types of ErrP have been identified based on the context in which the error occurs:

- **Response ErrP**: Generated after an incorrect motor action [58].
- **Feedback ErrP**: Generated only after making a decision. If the decision results in an error or the subject realizes they made a mistake, ErrP is generated [59].
- **Observation ErrP**: Generated after observing an external person make an error [60].
- **Interaction ErrP**: Generated when a BCI provides a command considered erroneous by the subject [61].

The shape of ErrP can vary significantly depending on the type of task a person is performing [62]. It can be a simple Error-Related Negativity (ERN) with a latency of about 50-100 ms in the case of an incorrect response [63]. Alternatively, it can be a broader complex of deflections, composed of an initial positive peak around 200 ms after a BCI feedback [64], a negative peak at 250 ms, a positive peak at 320 ms, and another negative deflection after about 400 ms [65], the previously mentioned N400. However, all these latencies are indicative and not constant values [66]. It should also be considered that ErrP amplitude is inversely proportional to the error rate present.

1.4 BCI classification

BCI technology is based on a closed-loop architecture (Figure 1.1), where mutual learning is fundamental [67]. Both agents, the brain and the machine, are stimulated for mutual learning [68]. The brain generates specific brain signals under precise conditions, while the machine,

through machine learning algorithms, comprehends and predicts the user's intentions, facilitating the transmission and classification of intentions [67]. Specifically, a features extraction step is necessary, wherein the essential features to describe the signal, such as amplitude, frequency, and peak latency, are defined. Subsequently, the extracted features are utilized to classify the user's brain signal and intention using machine learning algorithms. The classifier is trained on these features, allowing it to recognize future brain signals from the same individual. This adaptability is crucial as brain patterns are highly subject-specific. The concept of a closed loop is crucial as it allows the user, through feedback and reinforcement learning, to verify the machine's performance once the brain signal is classified [69]. Simultaneously, it enables the computer to correct its errors, modify its interpretation, and reach the user's actual intention [70]. The classification of BCI technologies refers to the technology used to access information on brain activity or the paradigm on which such technology is based.

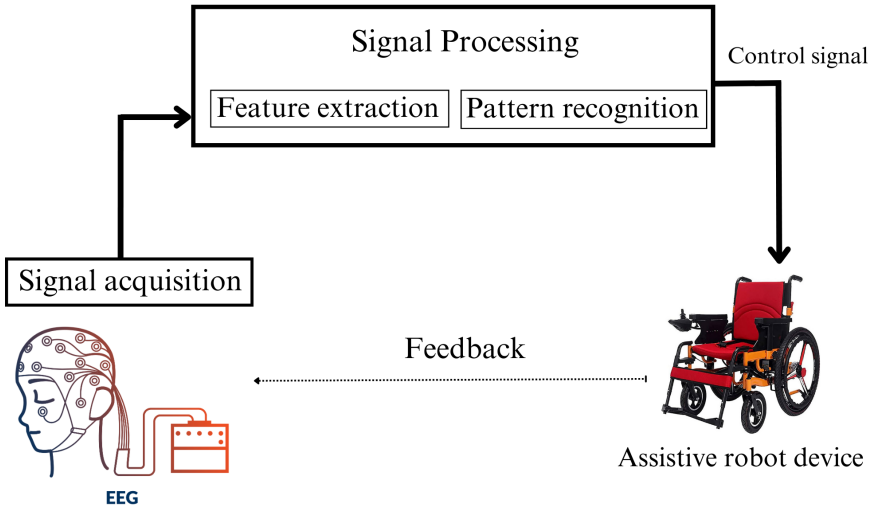

Figure 1.1: *BCI as closed loop*

1.4.1 Invasive vs. non-invasive acquisition techniques

To record brain signals, various technologies have been developed, which can be either invasive or non-invasive. A possible classification of BCI follows that of data acquisition technologies. It is essential to note that invasive BCI (based on ECoG) is only possible following a surgical operation to implant electrodes in close contact with brain tissue [71]. This makes it more expensive, risky, and ethically debated in the research field [72]. Several factors, such as the brain area to be investigated, the subject under examination, electrode biocompatibility, post-operation wound healing time, electrode sharpness, and electrode placement speed, must be considered before, during, and after implantation [73]. However, the data obtained have high signal-to-noise ratio due to limited impedance sources and proximity to the signal source [74].

It also provides high spatial and temporal resolution compared to non-invasive brain recording techniques [75]. This high precision is essential for accurately interpreting neural signals involved in decision-making and motor processes.
Non-invasive BCI, usually based on EEG, has reduced costs and is more easily implementable in various clinical and research contexts, making it the most widely used [76]. The main limitations include the large size of the electrodes, resulting in low spatial resolution, and the high impedance from the tissues between the brain and the electrodes [77].

1.4.2 Exogenous vs. endogenous BCI

Another possible classification is based on the two types of cerebral phenomena that can be exploited by the BCI. The first involves signals generated by external sensory stimuli, such as visual flashes or sounds, while the second involves internal voluntary decision processes, such as imagining movement. The BCI is called exogenous when relies on the first cerebral phenomenon; endogenous if the second phenomenon is elicited. One difference is that while exogenous systems usually present higher computational efficiency, require less training, and can be learned by a broader user base; endogenous systems require constant user attention throughout the task, which can be fatiguing and frustrating, [78]; its effectiveness lies in the ability to directly detect and interpret internal neural signals, providing a more natural and intuitive interface. This feature is particularly relevant in contexts where a complete lack of motor functions necessitates advanced alternatives for communication and device control [79].
Endogenous BCI is primarily used for Motor Imagery (MI) experiments and the control of assistive physical devices such as wheelchairs, robotic arms, and exoskeletons [80]. The uniqueness of this technique lies in highly subject-specific and differently modulated brain rhythms among different users. Consequently, the computer necessitates personalized training using individual EEG data. The imagination of movement in the case of MI-based BCIs is subjective and generates signals with characteristics that vary from individual to individual. Consequently, users need prior training to attempt to produce signals as similar as possible to those of other users, allowing the computer to recognize such a signal correlated with motor intention. Similarly, the inability of a subject to generate a signal with specific characteristics necessitates the creation of a subject-specific classifier.
In this case, endogenous signals such as SMRs and SCPs are mainly employed [37]. The main complication of this type of BCI is that the user must practice generating specific brain patterns that the computer can record and discriminate from other physiological signals, achieved through neurofeedback [81].
On the other hand, exogenous BCI exploits the passive and uncontrollable generation of brain signals by the user, resulting from external stimuli [82]. The goal is to decode evoked potentials

or event-related potentials generated by an external event. This type of BCI primarily relies on steady-state visual evoked potential (SSVEP), P300, and ErrP [83]. It is more easily implementable than the previous type because, for certain modalities like SSVEP, there is no need for extensive user training, and it often exhibits higher performances [84]. However, it is important to note that this may not be as straightforward for other modalities, and the ease of implementation can vary based on the specific type of exogenous BCI. In this case, as well, it is necessary to train a classifier to establish the presence of the sought-after signal. However, since this signal is spontaneous, the training margin for the subject is more limited and less demanding.

1.5 Related work

The integration of ErrPs in BCI systems is particularly interesting because it provides a way to detect and correct errors in the interpretation of the user's intentions. As BCIs rely on decoding neural signals to infer user commands, there is a possibility of misinterpretation. ErrPs can act as a feedback mechanism, allowing the BCI system to recognize errors in real-time and adjust its interpretation or actions accordingly.
As demonstrated in the experiment conducted by I. Batzianoulis et al. [85], the integration of ErrP with a BCI can lead to an improvement in the performance of an external device. Specifically, in the study, the ErrP was generated when a user observed the incorrect behavior of a robotic arm during its autonomous movement. The robot adjusted its trajectory to reach a goal, using ErrP as feedback. In this way, the movement of the robotic arm was optimized according to the user's intention, as the user judged a particular movement as incorrect.
Most of the studies in the literature focus on the analysis and implementation of ErrP in discrete control BCI.
Ferrez and Millan conducted an experiment investigating ErrP resulting from BCI command execution failures [86]. Participants manually transmitted cursor movement commands to prevent ErrP recognition issues caused by the classifier misinterpreting user MI. The system deliberately induced ErrP with a 20% probability by moving the cursor opposite to the user's intended direction. The study underscores the manifestation of ErrP due to BCI misinterpretations during a discrete control. The research, focused on the neural correlates of error awareness, aims to enhance BCI performance by identifying a unique ErrP type associated with the misrecognition of the user's intention. It provides valuable insights into BCI applications, demonstrating the potential for detecting single-trial errors and highlighting the stability of these potentials over time.
Unlike discrete control, there is a lack of studies in the scientific literature regarding the implementation of such a signal during continuous control of an assistive device. Providing users

with the ability to control a device continuously would increase the utility, convenience, and effectiveness of BCI technologies, bringing them closer to real-world scenarios.
An example of the use of ErrP during continuous control of a device is represented by the work of Catarina Lopes-Dias et al. [87]. During the experiment, ErrPs were asynchronously decoded in an online scenario, revealing the electrophysiology of the signal during both the calibration and online phases of the experiment. In both conditions, ErrPs exhibited similar shapes, but the overall average of ErrPs in the online condition showed higher peak amplitudes. The decision to display the electrophysiology of ErrPs in both conditions using EEG signals filtered with a causal filter deviated from the standard literature practice, which commonly employs a zero-phase filter. In the presented situation, the typical N200 component of ErrPs was shifted after the P300 component, a direct consequence of using a causal filter and not reflecting any peculiarities in neural activity (*Figure* 1.2). Lastly, it is suggested that providing participants with comprehensive feedback on ErrP detections would not only not diminish their performance but could potentially enhance it, considering the possible positive impact on their engagement and the hypothetical correlation with the observed increase in peak amplitudes of ErrPs in the online scenario.

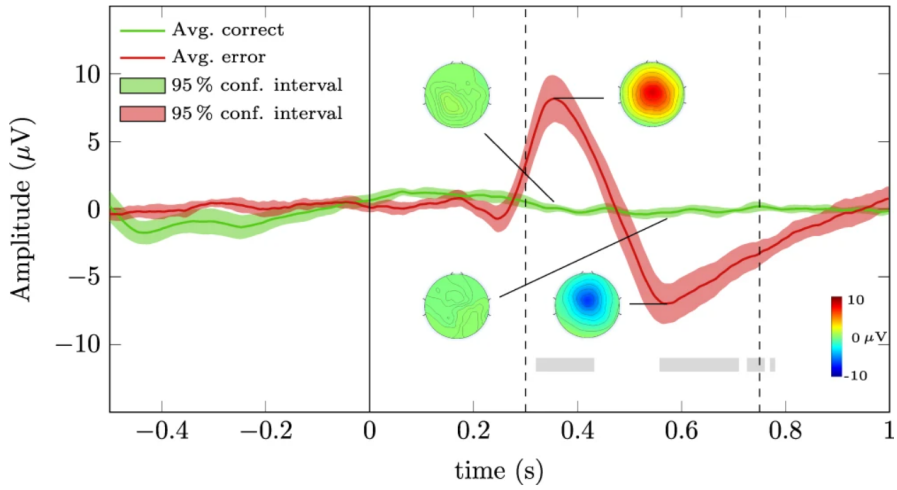

Figure 1.2: *Grand average correct and error signals at channel FCz (green and red lines, respectively). The green and red shaded areas represent the 95% confidence intervals of the grand average signals. The regions in which correct and error signals were significantly different are marked with a grey rectangle. The vertical line at t=0s represents the error onset of error trials and the virtual onset of correct trials. The dashed vertical lines at t=0.30s and t=0.75s delimit the window used to train the ErrP classifier [87].*

Another study is the work of Iwane et al. [66], which investigated the latency of Error Potentials when generated in predicted or unpredicted states during a continuous control protocol. Specifically, a cursor moved autonomously to reach a predetermined point and sometimes made errors related to the angle of traversal and the distance from the final goal. The subject had to

monitor and evaluate the cursor's trajectory until it stopped. The error related to the angle of traversal was classified as predicted because, once committed, reaching the final goal was not possible, and it could be evaluated how and when the error occurred. If the cursor did not reach the goal, despite the correct trajectory but stopped before or after the error, it was classified as unpredicted because it was more difficult to predict. Researchers demonstrated how the shape of Error Potentials, especially latency, varies from subject to subject and under different control conditions. For unpredicted errors, an increase in latency was recorded due to an increase in the user's cognitive processing. Furthermore, it was highlighted that the shape of the error potentials could undergo changes once data filtering was applied through a causal filter.
The ultimate goal of the scientific community is to develop a control device for users with irreversible damage to the upper and lower limbs but with still brain functionality. The use of a motorized wheelchair would allow individuals with mobility impairments to regain their independence and experience an improvement in their quality of life. However, in the current scientific literature, there are still no articles that integrate BCI technology with wheelchair control, also incorporating error detection management. An example of a study on a motorized wheelchair is represented by Tonin et al. [88].
This research aims to explore the hypothesis that the acquisition of BMI skills by end-users is crucial for the effective control of a non-invasive, thought-controlled intelligent wheelchair in real-world scenarios. The findings illustrate the successful training of three tetraplegic individuals with spinal cord injuries to operate a non-invasive, self-paced thought-controlled wheelchair, successfully executing complex navigation tasks. Notably, high navigation proficiency was attained only by the two users who demonstrated improved decoding performance, feature discriminancy, substantial neuroplasticity changes, and enhanced BMI command latency. The study further underscores the viability of achieving precise and continuous control of robots through a low degree of freedom, discrete, and uncertain control channel, exemplified by motor imagery BMI. This achievement is realized through the integration of human and artificial intelligence using shared-control methodologies.

1.6 Motivation and aims of the thesis

The study aims to assess the feasibility of recording the Error Potentials in the context of continuous control of a motorized wheelchair. The detection of ErrP assumes critical relevance as there are currently no specific applications for this type of assistive device based on BCI.
The objective is to identify the presence of the ErrP and describe its characteristics by comparing them with those previously studied in the literature, which has primarily focused on the ErrP during discrete BCI control.

Additionally, the ability to implement continuous control on an assistive device, thereby avoiding risks to the user's safety due to incorrect signal classifications by the machine, brings this technology closer to a real-world scenario. The control of a wheelchair is inherently continuous. The analysis conducted will contribute to the improvement of control system design for wheelchairs, providing guidelines for the development of broader applications of ErrP in continuous control contexts. This will enhance the safety and effectiveness of user-controlled robotic devices, solidifying the practical applicability of this technology in assistive settings.

Chapter 2

Methods

2.1 Subjects

9 subjects, 7 males, and 2 females, with ages between 22 and 26 and an average age of 24.1, participated in this study (*Table* 2.1). All subjects were healthy and were informed of the experiment's purpose and protocol before data acquisition. Informed consent was obtained from every volunteer who participated in the experiment.

Table 2.1: *List of participants in the experiment*

Subjects' List		
	Sex	Age
S1	M	26
S2	M	23
S3	M	25
S4	M	26
S5	F	23
S6	M	25
S7	M	25
S8	F	23
S9	M	22

2.2 Equipment

2.2.1 Powered wheelchair

The wheelchair used is the HI-LO VARIO model 18.70 from the manufacturer Vassilli, located in Padua, Italy. The wheelchair can be controlled by the user through a joystick located on the right armrest, but for this experiment, an external gamepad has been connected to customize

control and make driving more autonomous and convenient. Two motors drove the two front wheels, while the rear wheels were free. A metal rod was installed on the left armrest with a cross sign attached. The user had to keep their gaze on the cross throughout the entire run to minimize as much as possible the noise generated by the eye movements.

Figure 2.1: *Vassili's HI-LO VARIO wheelchair, model 18.70, used in the experiment*

2.2.2 Electroencephalography system

For the EEG data acquisition, the eego™ sports 64 headset produced by AntNeuro (Hengelo, Netherlands) was used. Out of the available 64 electrodes, 32 were utilized (Fp1, Fp2, F1, F2, Fz, Fc1, Fc2, Fc3, Fc4, Fc5, Fc6, FCz, C1, C2, C3, C4, C5, C6, Cz, Cp1, Cp2, Cp3, Cp4, Cp5, Cp6, P1, P2, P3, P4, P5, P6, Pz), due to the limited region of interest, in the standard 10-20 configuration [89] in addition to the electrode for recording electrooculographic (electrooculogram (EOG)) activity [90]. The headset was connected to the supplied amplifier via shielded cables. Each subject was asked to sit in the chair to allow the headset placement. Once the helmet was worn, the distance from nasion to inion and from the right to the left ear canal was measured using a tape measure, which was passed along the apex of the skull. The position of the Cz electrode was adjusted to coincide with the midpoint of the previously measured distances, ensuring the correct alignment of all other electrodes. To improve signal conductivity, a water and ion-based gel was applied through the 32 electrodes using a syringe. The EOG electrode was placed under the left eye using a strip of adhesive tape after applying a layer of

conductive gel to the metal surface. The ground electrode was placed in GND and the reference one in CpZ.

Figure 2.2: *EEG used during the experiment.*

2.3 Experiment protocol

The subject was instructed on the necessary commands for controlling the chair and the path to follow, which consisted of 3 right turns and 3 left turns with varying angles and durations. The path included obstacles such as 3 chairs with wheels and a column to navigate around. The experiment was considered complete once the subject had performed a total of 18 runs - 9 with continuous control and 9 with discrete control. The first run for both control types served as a 'practice' run and did not involve induced errors, unbeknownst to the subject. The experiment proceeded by alternating two runs with continuous control and two runs with discrete control until completion. This thesis exclusively examines the continuous driving mode for wheelchair control, and henceforth, only this control mode will be taken into consideration from now on.

2.4 Wheelchair control

2.4.1 Communication middleware

A set of software libraries, referred to as the Robot Operating System (ROS) [91], was implemented to enable communication and ensure synchronized recording of data from the three distinct hardware components (joystick, motorized chair, EEG headset). This framework facilitated interaction between the joystick and the motorized chair, allowing efficient transmission of user commands. The commands were sent to the wheelchair, where they were processed and

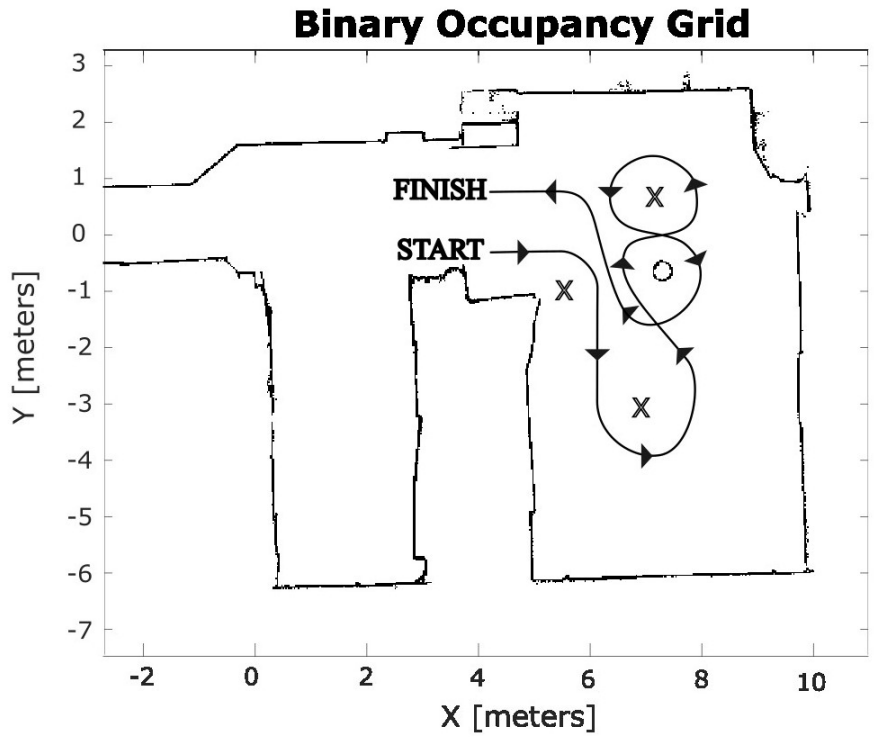

Figure 2.3: *Map of the laboratory where the experiments were conducted. The black line indicates the path that each subject had to follow, and the black arrows indicate the direction of navigation. Xs are the chair while the circle indicates the column*

converted into velocity signals. Thus, ROS allowed to manage four different types of data (joystick input, wheelchair velocity, wheelchair odometry, EEG signals) from three distinct hardware systems. This integration played a decisive role in synchronizing a substantial amount of diverse data.

Specifically, the synchronization between the wheelchair's velocity and the data from the EEG headset was managed through ROS-Neuro: an open-source framework based on ROS for neurorobotic applications [92]. This aspect is crucial for extracting EEG trials containing errors, as a specific event was recorded at the temporal instance when an induced error occurred during driving.

Moreover, ROS has proven instrumental in managing correct trials and evaluating the delay, a temporal interval that will be described later in section 2.5.3. Utilizing the odometry of the chair, specifically the angular velocity which allowed the determination of the onset of a curve, was essential for extracting the trials without the induced error.

2.4.2 User command

Wireless control was performed through the Logitech F710 gamepad connected to the laptop located at the rear of the wheelchair. The protocol developed exclusively required the use of the right analog stick to control linear and angular speed and a button to halt navigation in case of emergency. The wheelchair control was implemented by initially taking the joypad's analog stick's position as input, representing a point with xy coordinates in a 2D plane. In this plane, the x-axis represents angular velocity, and the y-axis represents linear velocity. The position of this point was confined within a unit circle centered at the origin. A vertical section of a right circular cone with two sides was defined within this circle to ensure a clear distinction between linear and angular velocity components. These values were then scaled to ensure safe and satisfactory chair control for the user.

There are three possible control conditions as shown in *Figure* 2.4:

1. *Straight*: the analog stick is positioned within the cone section, resulting in only linear velocity (no reverse velocity).
2. *Turn*: the analog stick is outside the cone, introducing an angular velocity component.
3. *Stop*: as long as the "B" button is pressed, the chair remains stationary.

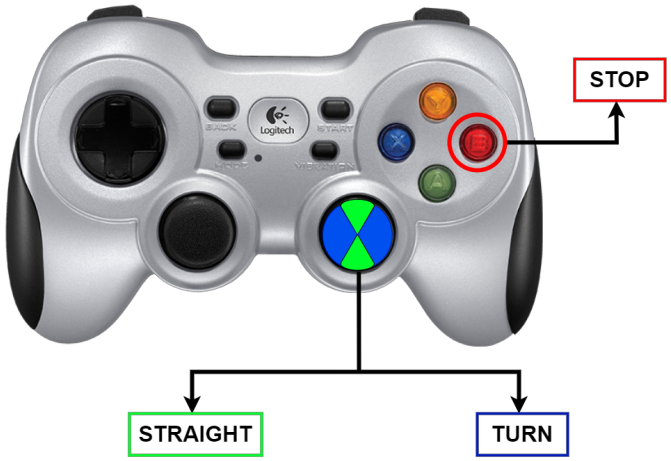

Figure 2.4: *Joystick used during the experiment. The three different control conditions are highlighted*

During the command execution process, a temporal delay in EEG data emerged, as a result of the interaction of various variables. These factors include the transmission time of the command from the joystick to the chair, the period required for the effective execution of the command, the initial position and velocity of the chair, the promptness with which the user perceives the

transition from a *Straight* condition to a curve (”Turn”), the angle of curvature chosen by the user, and the adopted driving style. It is crucial to emphasize that the temporal shift represents a highly subject-specific measure. Consequently, a delay measure has been calculated for each user as explained in section 2.5.3.

2.4.3 Error generation

To induce navigation errors and record the Error Potential, the duration of the path was pre-estimated to be 2 minutes. At the beginning of each run, a random number of errors, ranging from 1 to 4, is generated. The limitation on the number of errors has been introduced to prevent the user’s expectation regarding the generation of induced errors. Furthermore, in the case of a high and unrestricted number of errors over multiple sessions, there is a risk that the subject may misinterpret the absence of induced errors as an error, rather than recognizing it as a command executed correctly by the wheelchair. The estimated run time is divided into intervals equal to the number of errors that will occur. An error is generated in each of these identified intervals at a random time.

The occurrence of induced errors depends on the wheelchair’s condition:

Condition 1: If the wheelchair is in condition *Straight*, the error occurs as soon as the control exits the cone and enters the curve phase.

Condition 2: If the wheelchair is in condition *Turn*, the error occurs only after the analog stick re-enters the cone and exits it again.

Condition 3: If the wheelchair is in condition *Stop*, the error timing depends on the user’s command immediately after exiting this condition, with reference to the previous points a and b.

The induced error consists of reversing the angular velocity of the curve compared to the input provided by the user for X seconds with fixed acceleration.

2.5 Data analysis

The dataset consists of two separate files: a gdf file containing EEG data and a bag file containing wheelchair odometry data. Data processing was performed using MATLAB R2022a.

2.5.1 GDF processing

For each run of each subject, the initial and final 3 seconds of data were removed to avoid transients during data concatenation. Out of the initial 32 channels, only the 10 significant

channels (FZ, FC1, FC2, CZ, CP1, CP2, PZ, FCz, C1, C2) were retained for the investigation of the specific brain area. To demonstrate that eye movement did not influence the extraction and classification of Error Potentials, three distinct analyses were subsequently conducted:

(a) Raw analysis: Since ErrPs are relatively slow potentials [93] a 4^{th} order Butterworth causal bandpass filter with a frequency range of [1, 8] Hz was applied

(b) CAR analysis: Filtering as point (a) and then a spatial filter was applied, using the common average reference (CAR) [94]. For each *Error Trials*, a delay was computed as will be explained in section 2.5.3, and applied to them, intending to align temporally the peaks of the ErrP.

(c) AMICA analysis: A 4^{th} order Butterworth causal bandpass filter with a frequency range of [1, 45] was applied. The use of a wide range of frequencies is justified by the need to initially retain high-frequency components not attributable to EEG signals, particularly ocular signals, which typically fall within the frequency range of 0 to 50 Hz [95]. This procedure was essential for subsequently conducting the Adaptive Mixture of Independent Component Analysis (AMICA) [96] and accurately identifying and separating all components contributing to the raw EEG signal. The components visually attributable to artifacts of various nature (eye movements, muscle movements, heart rate, noise channel, line noise) or exhibiting patterns not resembling a brain signal were removed. Subsequently, the signal was reconstructed considering only the remaining components. Finally, a bandpass filter and a spatial filter were applied as in point (b). For each *Error Trials*, the instant of the negative peak of the Error Potential was identified. This peak was subsequently shifted to 0.4 seconds to allow for a comparison of the shape and latency with the literature.

For each analysis, the individual runs were concatenated without including data from the EOG electrode, which was stored in a separate variable.

Trials related to errors, referred to as *Error Trials*, were extracted considering a time window of 1.5 seconds, starting from 0.5 seconds before the occurrence of the error until 1 second after. Trials related to moments without errors called *Correct Trials*, consisted of 1.5 seconds of data starting from the transition from the Straight to Curve condition when no induced error was present. Similarly, trials, both *Correct* and *Errors*, related to the EOG signal were extracted, called *EOG Trials*.

2.5.2 Statistical Analysis

For each signal resulting from the three analyses described above, the correlation between all EEG and EOG trials (Correct and Incorrect) was calculated. A Analysis of Variance (ANOVA) was applied to assess the independence of each signal from the other two, using a significance level alpha equal to 0.5.

2.5.3 BAG processing

The wheelchair odometry was used to extract the *Correct Trials* beginning time: the instant when the wheelchair enters the *Turn* condition was recorded as the time required to reach a predetermined angular velocity chosen empirically, called *Turn Velocity* reflecting the speed at which the user realizes the *Turn* condition has been reached. This instant was sent to the GDF file for the extraction of the *Correct Trials*.

Similarly, the signal shift value over time called *Delay*, has been extracted. In this case, two instants were considered: one related to the delivery of the command and the other related to the achievement of the *Turn Velocity*. It is worth noting that induced error can occur only after transitioning from a *Straight* condition to a *Turn* condition. The difference between these two instances constitutes the *Delay*.

The calculation of the *Delay* was not necessary for the *Correct Trials* due to the particularly flat EEG waveform without fluctuations in this context.

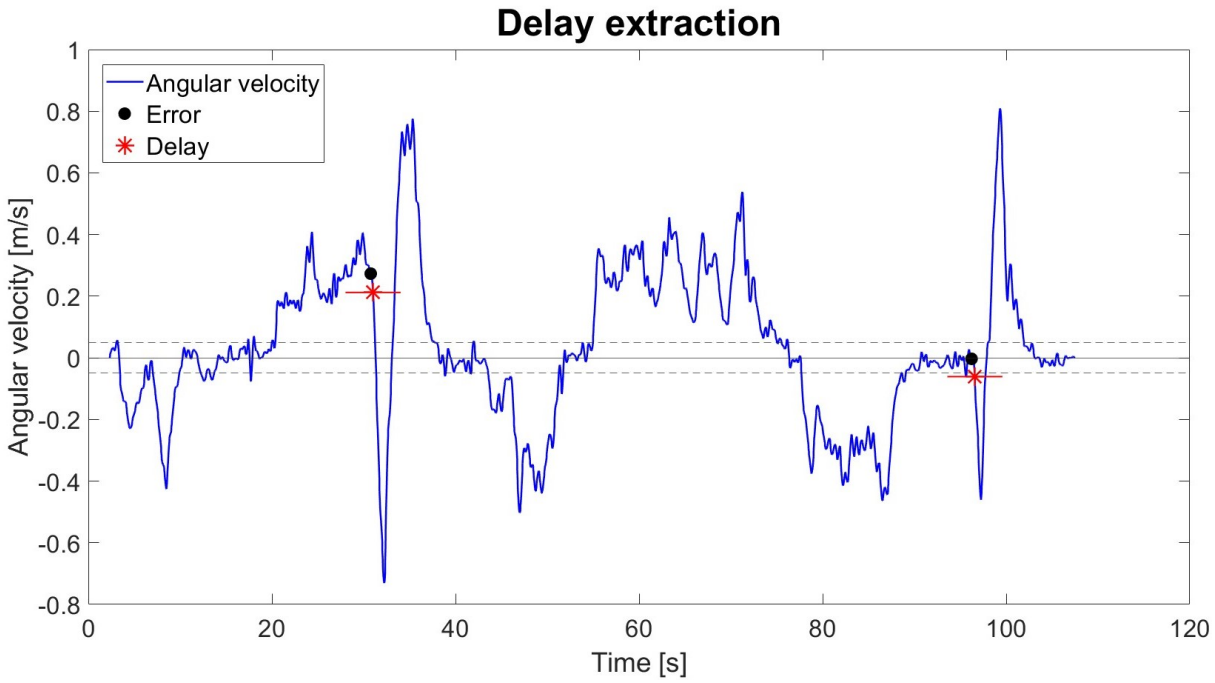

Figure 2.5: *The blue line is the wheelchair's angular velocity, the black points are the instants at which the error-induced commands are generated, and the red stars are the delays calculated. The dashed lines at ± 0.05 refer to the empirical angular velocity at which the user realizes that is in the Turn condition*

Chapter 3

Results

The following chapter presents the results of the analyses conducted. The images related to the EEG signal specifically refer to the FCz channel.

3.1 Eyes movements

Of all the possible different physiological artifacts influencing an EEG signal, herein, only those related to eye movement were considered. In a driving context such as that outlined in the thesis, it is natural to observe participants exhibiting ocular movements. The predetermined path, the presence of obstacles along the route, and the unfamiliarity of the environmental context in which the subjects found themselves, compounded by the novel experience of operating a motorized wheelchair, collectively influenced ocular behavior. Despite pre-experimental instructions to fixate on a sign placed in front of the wheelchair, individuals exhibited a lack of consistent gaze fixation. *Figure* 3.1 depicts the comparison of average EOG and EEG signals during the *Error Trials* for subject S8. Signals are both filtered with a fourth-order causal bandpass filter in the frequency range of [1-8] Hz and no spatial filter was applied. From *Figure* 3.1, it can be observed that the EEG signal of *Error Trials* follows the same trend as the EOG, confirming the hypothesis of a strong presence of ocular artifacts in the cerebral signals.

A CAR filter has been applied to remove ocular components. *Figure* 3.2 shows the EOG and EEG signals related to the *Error Trials* for two distinct subjects, S8 and S1, to highlight the different results after the application of the spatial filter.
As can be seen in *Figure* 3.2 after the application of CAR, non-uniform results were obtained among these two subjects. On the one hand, in the case of S1, one can observe a qualitative difference in the EEG signal compared to the EOG, by examining the position and amplitude of the peaks. On the other hand, for subject S8 the EEG signal exhibits a similar waveform to the EOG signal, with the only distinction being in amplitude. The positive and negative peaks

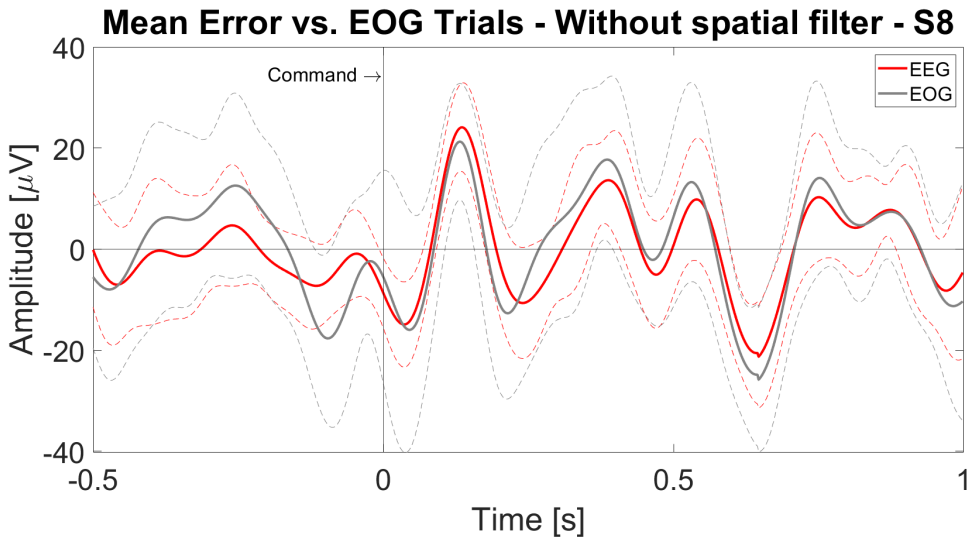

Figure 3.1: *Mean with standard deviation (dashed line) of the EEG signal (red curve) and the EOG signal (grey curve), related to the Error Trials for channel FCz. At 0 seconds (vertical black line) it's the beginning of the condition Turn*

are aligned, suggesting a close correlation between the two signals. This lack of uniformity is probably due to the subject-specific behavior during the navigation task and it affects all the participants in the study.

Since the CAR filter was not able to remove the eye influences in all the subjects, it was decided to perform an AMICA analysis. AMICA was also used to remove artifacts originating from other sources (muscle, heart rate, hardware noise, etc.). *Figure* 3.3 shows a visually different signal following the removal of the noise components.

To quantitatively assess the influence of eye artifacts in raw signals, CAR-filtered signals, and signals obtained through the combination of CAR and AMICA, cross-correlation between EEG (electrode FCz) and EOG signals was calculated.

Figure 3.4 reports the distribution of the correlation values for all the subjects in the three aforementioned conditions. Results show that the correlation between EEG and EOG signals without any spatial filter is very high (median is equal to 0.84). Applying CAR filter reduces this correlation, resulting in a median value of 0.43. The further application of **ICA!** (**ICA!**) decreases this value (median = 0.29), indicating the low influence of eye artifacts in the filtered signals.

To assess the statistical differences in correlation indices among the three cases under analysis, an ANOVA test with Bonferroni correction was conducted. The presence of the asterisks in *Figure* 3.4 indicates the statistical difference with a significance level of 0.05 from ANOVA results.

Subsequently, a subject-specific cross-correlation analysis was conducted. The results revealed that in only 2 out of 9 subjects (S6 and S8), the correlation between EOG signals and

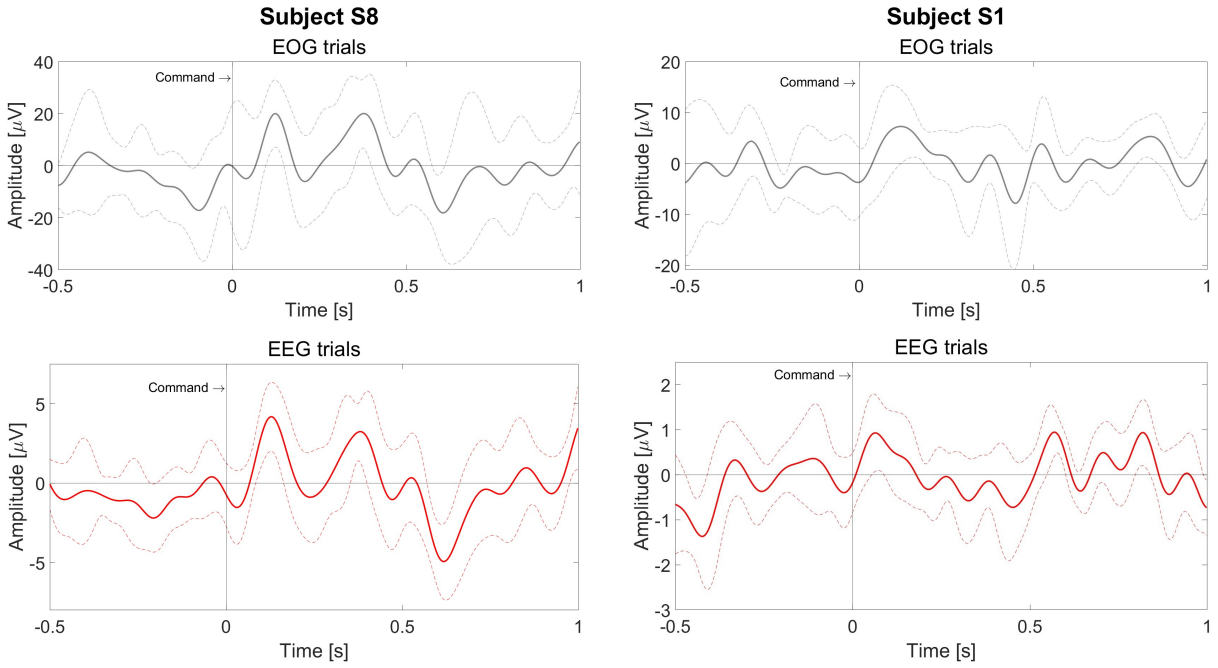

Figure 3.2: *Mean with standard deviation (dashed line) of EOG (grey line) and EEG (red line) signal filtered with CAR. Signals are related to Error Trials for S8 (left) and S1 (right). The black vertical line indicates the beginning of the condition Turn*

CAR-filtered EEG signals was high (median > 0.5). This highlights that the CAR filter removes the ocular component in most of the subjects.

Comparing the results between the CAR-filtered signal and the signal filtered with both CAR and AMICA, a decrease in correlation values was observed for all subjects, except one (S9), where the median correlation values were 0.40 and 0.45 in the respective analyses. This demonstrates that the application of AMICA further removes components related to eye movement and other sources of noise, making the signal cleaner.

Figure 3.5 presents the results for three subjects, while the remaining results are provided in the Appendix A. For S1, it is observed that the application of the CAR filter and the CAR filter in combination with AMICA progressively reduces the ocular component. S8, on the other hand, shows that spatial filtering alone does not eliminate the influence of the eyes, while the additional application of AMICA achieves this effect. For S3, cross-correlation values are similar and low for all analyses, indicating a low initial influence of the eyes on the signal.

The statistical ANOVA test was conducted to assess significant differences, and the results are presented in the *Figure* 3.5 using asterisks to identify statistically different groups with a significance level of 0.05.

It is therefore evident that ocular influence is subject-specific and only for some subjects it has an impact on the EEG signal despite the application of the CAR filter. Nevertheless, it has been decided to proceed with the analysis using the CAR filter and the application of AMICA

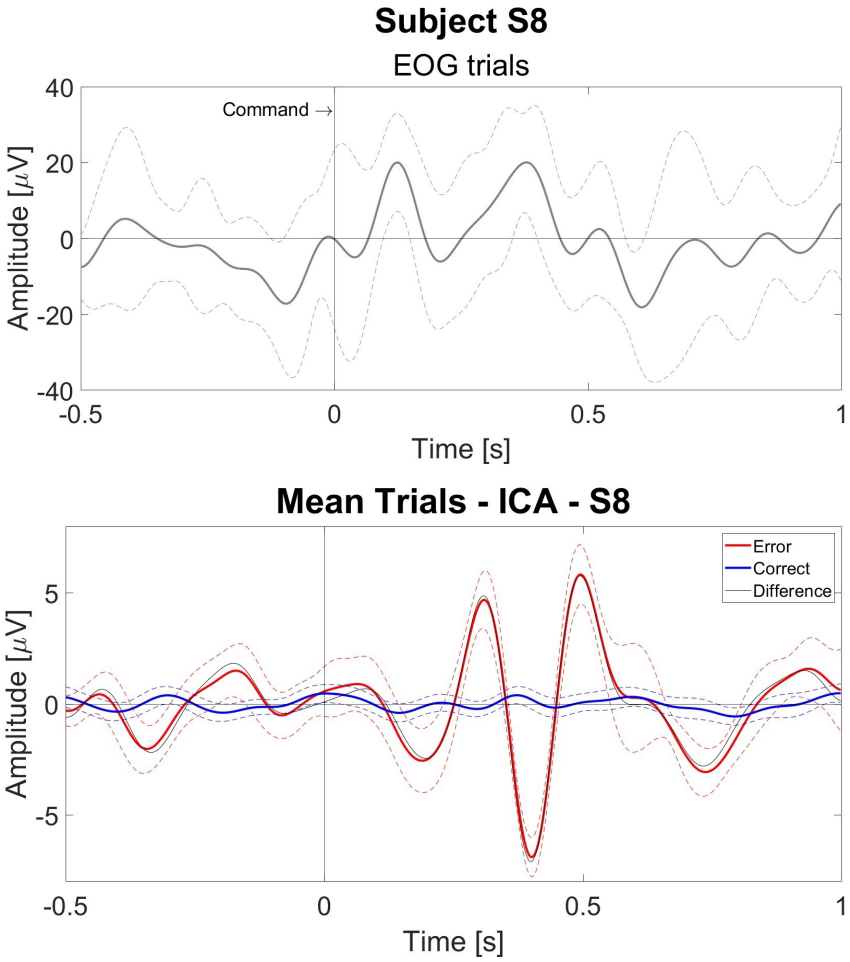

Figure 3.3: *Top: the EOG mean signal with standard deviation. Bottom: the EEG mean with standard deviation after the application of CAR and AMICA. The time window refers to the Error Trials for S8. The black vertical line indicates the beginning of the condition Turn*

to extract the ErrP from signals where the artifacts' influence is the lowest.

3.2 Delay results

The ErrP is a signal associated with the perception of an error; as such, its occurrence varies for each individual by nature. The moment at which it is generated is not fixed but influenced by subjective factors. Furthermore, in the driving context described, the transmission of the command to the wheelchair occurred with a delay due to physical factors. In the Methods section 2.5.3, it was explained how the *Delay* was calculated by considering the angular velocity of the wheelchair and how it depends on subjective factors (driving style, attention, subject's weight) and objective factors (position of the wheelchair wheels, speed, command transmission time). Therefore, the computation of a delay was necessary to understand the instant at which the user

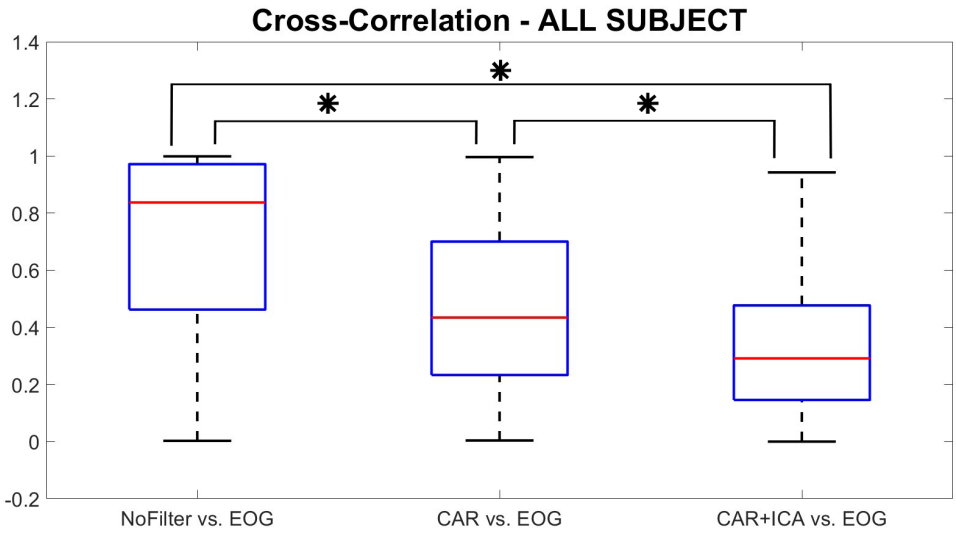

Figure 3.4: *Cross-correlation indices for all subjects related to all trials (Errors and Correct) of the EEG signal without CAR filter, with CAR filter and with CAR filter and AMICA vs. EOG signal. The asterisk means that the two corresponding correlation values are statistically different*

perceived the induced error. *Figure* 3.6 reports the average delays with standard deviation for each subject.

The average delay among all subjects is 0.274 ± 0.097 seconds. The use of these delays had initially been hypothesized to shift each *Error Trials* to achieve a temporal alignment of peaks capable of qualitatively highlighting the ErrP. It was thus applied to the CAR filtered signal of each subject. *Figure* 3.7 shows of which two examples are provided.

In the signal of S2, after the application of the delay, a clear ErrP-shape appears, and the negativity is present at 0.19 seconds. However, this result has not consistently been achieved, as seen in the case of S1, where the shift of the signal does not allow the identification of an ErrP. The averages of *Error Trials* for each subject were analyzed to assess the presence of ErrP after the introduction of the delay in the signal. All the other results are reported in Appendix A.

As the application of delay to CAR-filtered signals did not yield satisfactory results for identifying the ErrP, it was decided to manually align trial-by-trial the signal filtered with CAR plus AMICA. Manual shifting was performed to position the negativity of the ErrP at 0.4 seconds to obtain its characteristic shape. The average shifts for each subject are depicted in *Figure* 3.8.

It can be observed that the shifts exhibit greater variability compared to the delays extracted from angular velocity.

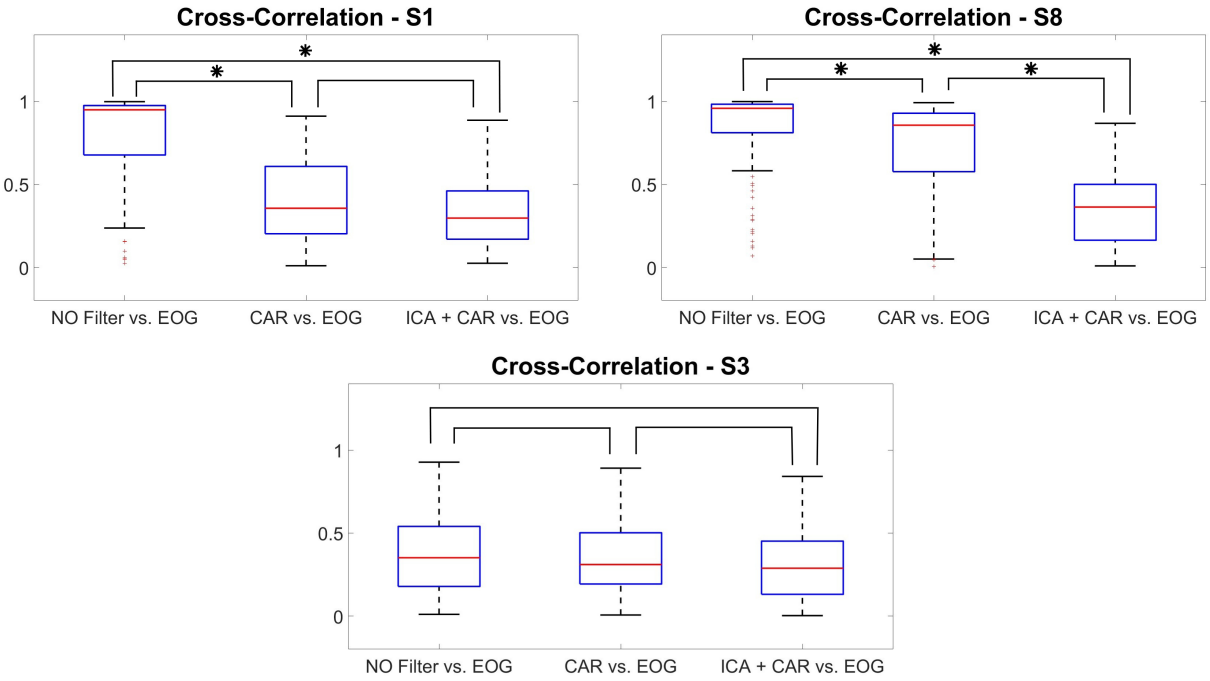

Figure 3.5: *Cross-correlation indices for S1, S8, and S3 related to all trials (Errors and Correct) of the EEG signal without CAR filter, with CAR filter and with CAR filter and AMICA vs. EOG signal. The asterisk means that the two corresponding correlation values are statistically different*

3.3 Grand average analysis

Since the goal of the thesis is to verify the presence and characteristics of ErrP during continuous control of a motorized wheelchair, it was decided to analyze the signal after AMICA to remove artifact components. Following the manual shifting of the negativity to 0.4 seconds, the signals obtained show the ErrP shape. The results of S1, S3, and S5 are depicted in *Figure* 3.9 and the others are in Appendix A. The figure shows the trend for *Correct* and *Error Trials* in the 1.5-second window of interest highlighting the two different brain responses to the external stimuli.

The negativity is present in every subject, but the amplitude varies from subject to subject. On the other hand, the two positive peaks are highly variable both in terms of amplitude and the timing at which they occur.

The average for all subjects of *Error* and *Correct Trials* is shown in *Figure* 3.10.

From *Figure* 3.10 is possible to distinguish three main peaks in the *Error Trials*:

1. **First positive peak**: at 0.3 seconds a positive peak appears with an amplitude of $1.20\mu V$
2. **Negative peak**: at 0.4 seconds a negative peak is present with an amplitude of $-4.25\mu V$
3. **Second positive peak**: at 0.5 seconds a second positive peak is present with an amplitude of $2.13\mu V$

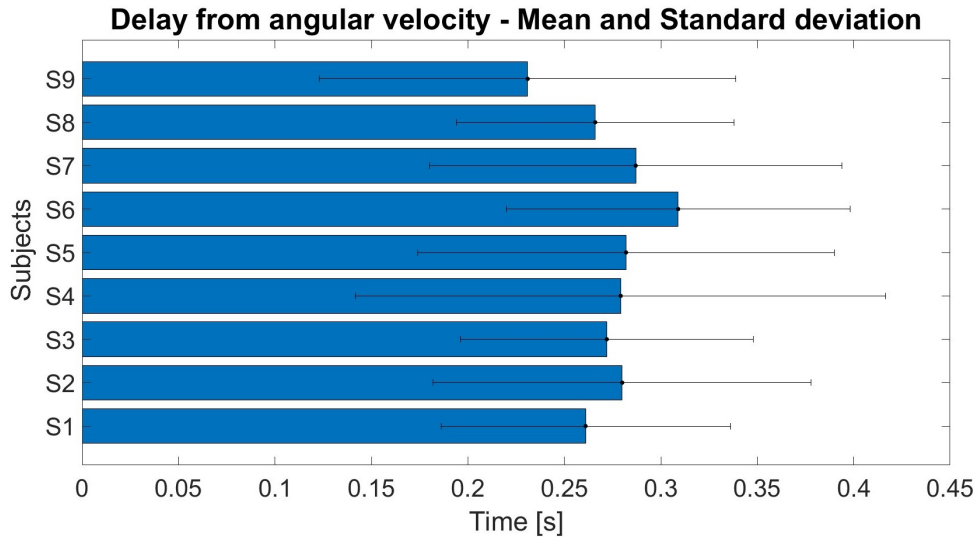

Figure 3.6: *Mean and standard deviation of the delay evaluated via angular velocity for each subject.*

The distinct brain response between the two classes of trials (Incorrect and Correct) is also highlighted by the topographic representation as shown in *Figure* 3.10.

A comparison was conducted with a similar study during the discrete control of the powered wheelchair in order to assess differences and compare the waveform associated with the two different control strategies. Results were analyzed cohesively in the continuous control study. Consequently, the signals were filtered through the application of a CAR filter followed by AMICA and appropriately shifted so that the negative peak of the ErrP aligned at 0.4 seconds.

From the visual analysis of *Figure* 3.11, the three peaks previously identified with continuous control are distinctly discernible:

- **Positive peak**: at 0.3 seconds, with an amplitude of $2.28\mu V$
- **Negative peak**: at 0.4 seconds, with an amplitude of $-4.20\mu V$
- **Positive peak**: at 0.5 seconds, with an amplitude of $1.29\mu V$

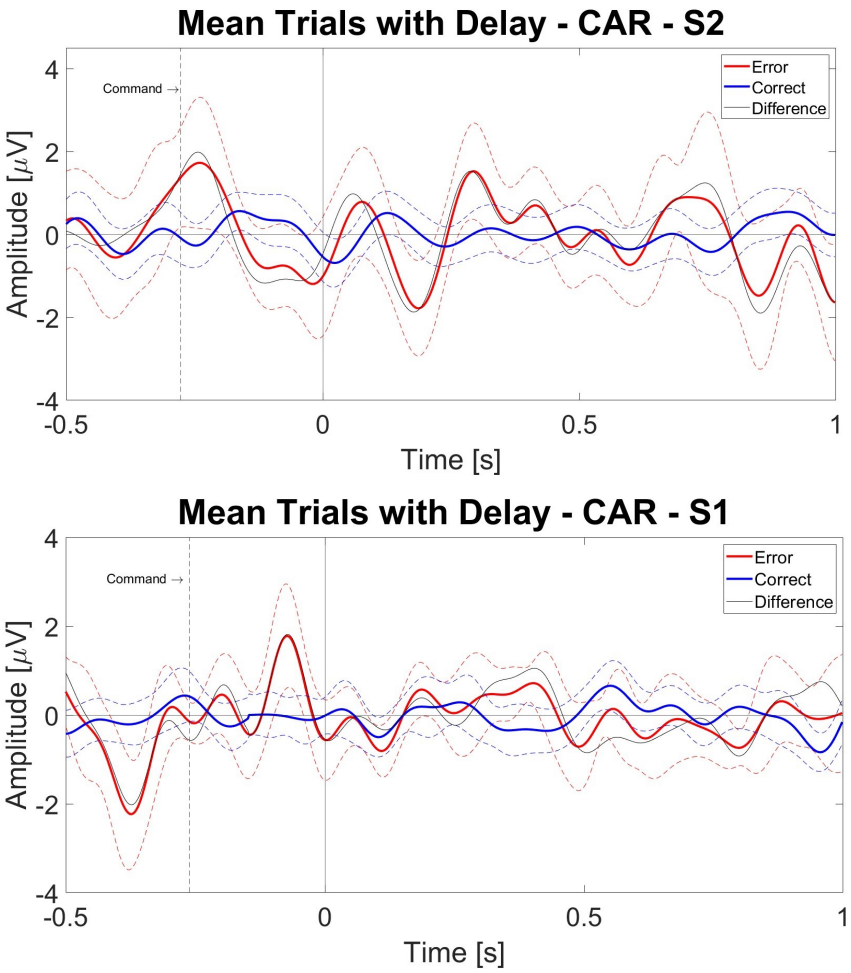

Figure 3.7: *Top: average with standard deviation Correct and Error Trials for subject S2, where ErrP is visible. Bottom: average with standard deviation Correct and Error Trials for subject S1, where no ErrP is present. The vertical black line at t=0s indicates the moment when it is hypothesized that the user perceives the occurrence of the induced error.*

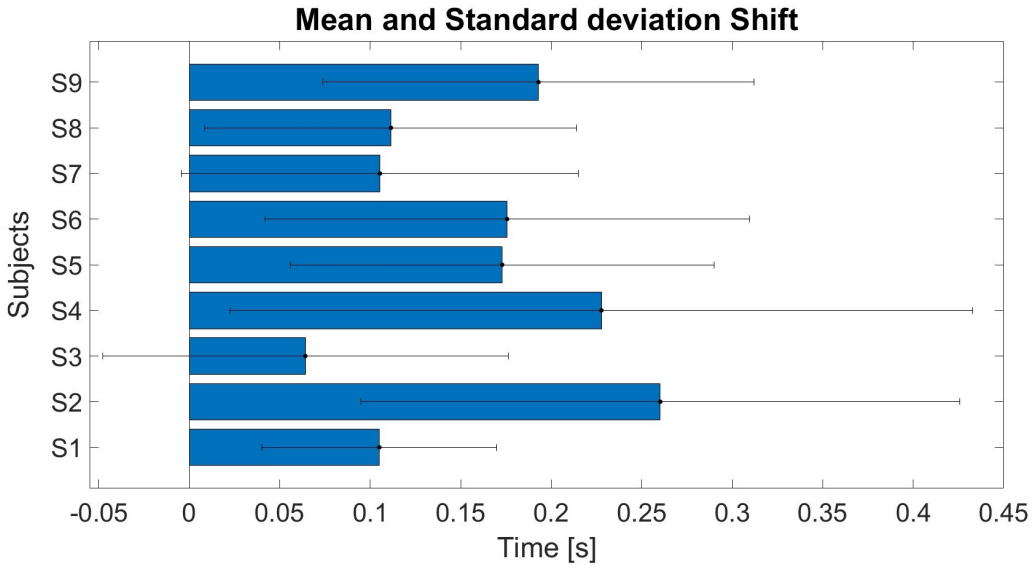

Figure 3.8: *Mean and standard deviation of the delay evaluated via angular velocity for each subject*

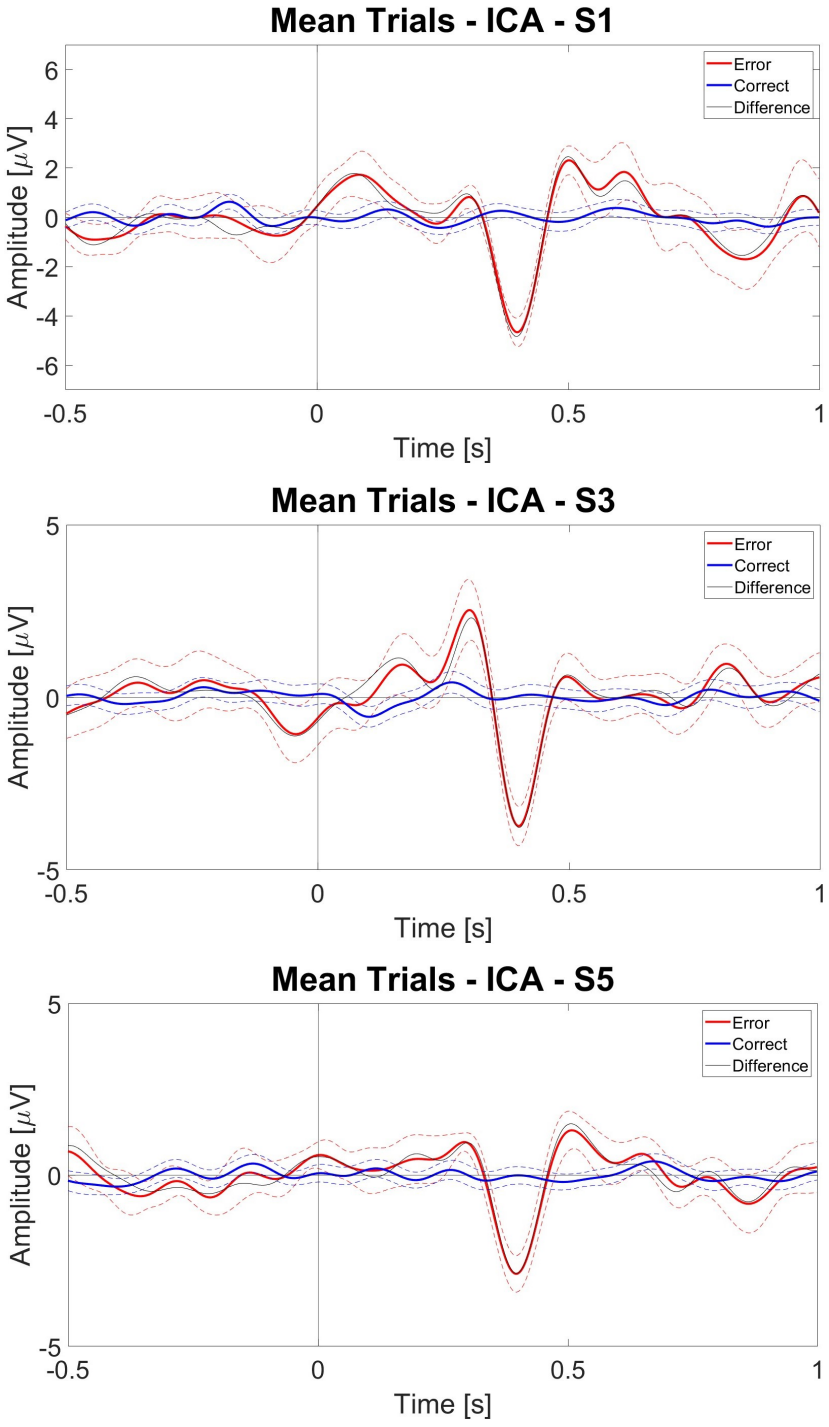

Figure 3.9: *Average with standard deviation of Correct and Error Trials (blue and red lines, respectively) at channel FCz for S1, S3, and S5. The signals were previously translated to manually align the negative peak of the Error Trials at 0.4 seconds.*

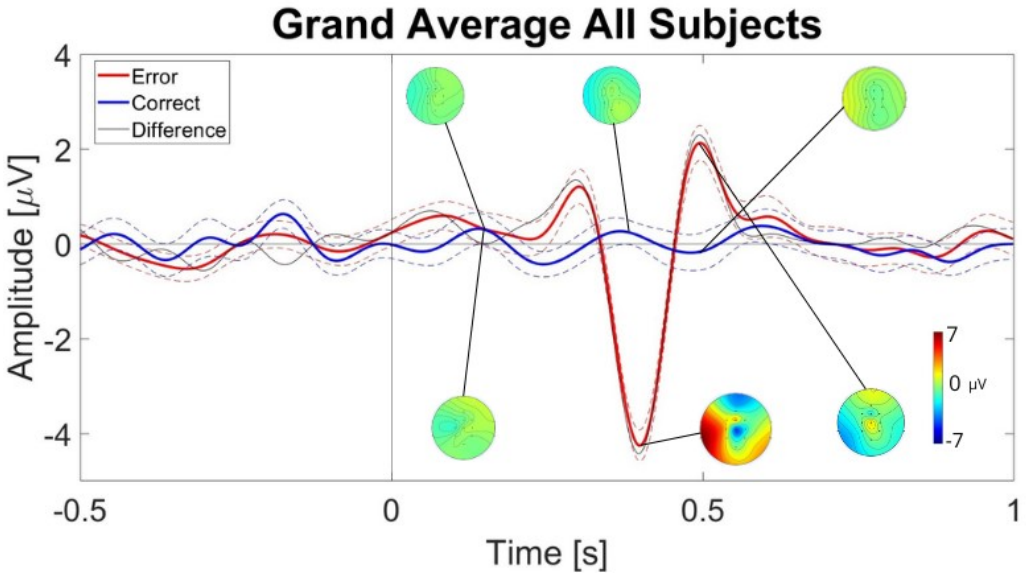

Figure 3.10: *Average with standard deviation correct and error signals at channel FCz of every participant (blue and red lines, respectively). The signals of each subject were previously translated to manually align the negative peak of the Error Trials at 0.4 seconds.*

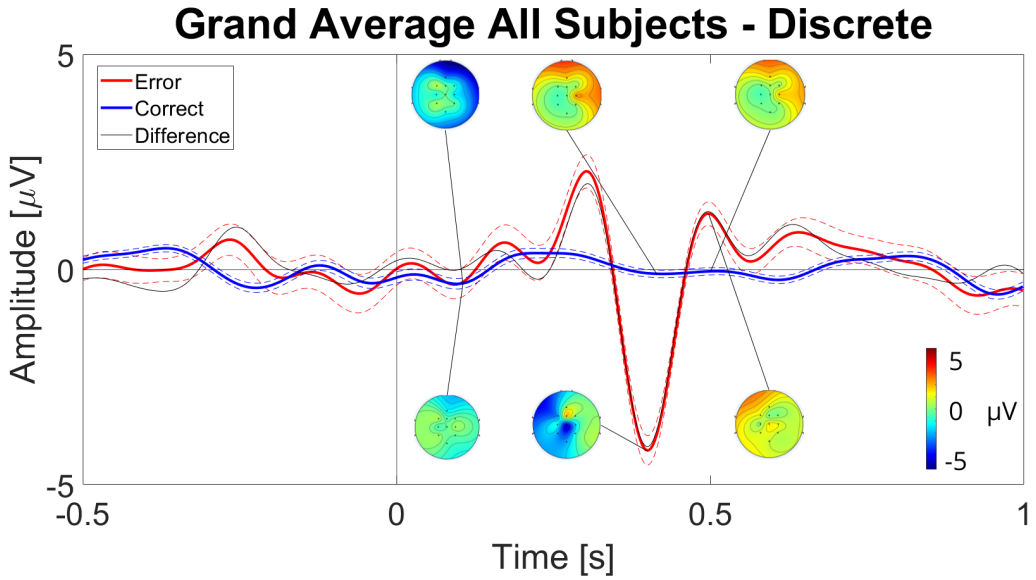

Figure 3.11: *Average with standard deviation correct and error signals at channel FCz of every participant (blue and red lines, respectively) in an experiment with discrete control of the wheelchair. The signals of each subject were previously translated to manually align the negative peak of the Error Trials at 0.4 seconds.*

Chapter 4

Discussion

.

4.1 Eyes movements

Before the experiment, participants were instructed to minimize movements and focus on a signal placed in front of the wheelchair to reduce ocular artifacts. Nevertheless, it was found that one of the most important disturbances to the EEG signal was related to eye movement. *Figure* 3.1 illustrates how the EEG signals exhibit a similar trend and amplitude to the ocular components recorded by the EOG electrode. This phenomenon can be attributed to the nature of the experiment, which involved a driving task for which the user had no prior experience. Furthermore, the route was not free, but rather well-defined, with the presence of obstacles requiring the user to make eye movements to avoid them. This led to eye movements during the driving task.

For the removal of ocular artifacts, a CAR filter was implemented, which eliminates components common to all EEG signals. The performance of the filter was satisfactory for most of the subjects in removing the eye components. From the visual inspection, for the other subjects, the influence of the eyes is still present (*Figure* 3.2, S8). This could be attributed to the fact that:

1. In cases where the eye component was present only in a few electrodes, the filter failed to remove that component as it was not considered common.

2. If the eye component was too high, the filter failed to remove it.

Since CAR did not remove all ocular components, it was decided to apply AMICA to further eliminate other interfering components, such as muscle movements, heartbeats, line noise, and channel noise. From a visual inspection (*Figure* 3.3), it can be appreciated that for S8, the trends

of the EOG and EEG signals are different. This confirms that AMICA is an effective method for removing noisy components from the signal.

As described in the *Results* the evaluation of ocular component removal was conducted. From the results of the cross-correlation (*Figure* 3.4), both methods reduced the eye influence. From the average analysis between all subjects, it follows that CAR is sufficient to remove artifacts from the signal.

From the analysis of single-subject cross-correlation (*Figure* 3.5), it emerges that CAR does not always yield satisfactory results, confirming what was observed in the previous qualitative analysis.

Another observation that has emerged is that for S5 and S3 (the latter illustrated in *Figure* 3.5), the correlation was already absent even before the application of the CAR filter. The explanation could be that these two subjects exhibited minimal eye movements during the experiment, minimizing the ocular influence on the brain signal.

Finally, the single subject correlation results indicate that the correlation between the signal filtered with CAR followed by AMICA and EOG signal is low for each subject. This justifies the use of AMICA in the search for the ErrP signal, as this analysis ensures greater signal cleanliness.

This is due to the lack of relevant studies on continuous control; the primary objective of this thesis is therefore to verify the presence of ErrP and characterize its form under the most convenient conditions possible.

However, implementing this technique online is impractical, necessitating the development of an alternative method for ocular artifact removal. One possibility is pre-experiment eye movement recording to create a subject-specific model. Nevertheless, online implementation of this technique remains challenging, and in a real-world driving context, it is not guaranteed that all ocular components will be correctly classified, potentially leading to issues.

4.2 Delay discussion

The calculation of the delay through the analysis of angular velocity has emerged as non-optimal for the ultimate goal of the thesis. Figure 3.6 shows that such delay is very similar among different subjects. Initially, this result was interpreted positively, as relatively low and consistent delays were obtained across subjects, as expected. This assessment was motivated by continuous control, as opposed to discrete control, allowing the user to maintain constant control over the wheelchair's position, speed, and acceleration, making them more attentive and sensitive to possible externally induced changes in these parameters. Consequently, it was hypothesized that any errors generated would be promptly recognized. Additionally, since each user traversed

the same path the same number of times under identical conditions, a very similar delay was anticipated across subjects.
However, it emerged that the introduction of the calculated delay was not functional. The classic waveform of ErrP was not recognized in all subjects, as shown in Figure 3.7. The average of erroneous trials in S2 exhibits a characteristic negativity associated with the ErrP, whereas such negativity is not observable in S1 after the introduction of the delay. This suggests that the delay is a subjective phenomenon, underscoring the need for a subject-specific universal metric to calculate it. The motivation for this observation could be attributed to the significance of subjective parameters, such as the user's weight, attention during the experiment, and driving style. These parameters were not quantifiable for a generalized analysis across all subjects.

Since the delay calculated through angular velocity did not yield satisfactory results for all subjects, it was decided to introduce a subject-specific manual temporal shift based on aligning the negative peak of the ErrP at 0.4 seconds of the signal with AMICA. The rationale for the ultimate use of the signal filtered with CAR plus AMICA is presented in the next section.

Referring to the average shifts for each subject (*Figure* 3.8), it emerged that the moment when the error is perceived varies significantly among subjects. Furthermore, the wide standard deviation suggests high intra-subject variability across trials. This is hypothesized to be attributed not only to individual factors such as weight and driving style but also to experimentally varying factors like attention level, error habituation, error expectation, which influence the user's error processing time. The aforementioned observation further justifies why the universal delay calculation used did not prove effective.

4.3 Grand-Average discussion

Given the scarcity of literature on ErrP identification during continuous control, especially in the context of wheelchair driving, where the waveform is not well-established, the analysis was performed on signals filtered with AMICA. This was done to mitigate the influence of signals originating from sources other than the brain that could potentially distort the characterization of the ErrP.

As highlighted in the *Figure* 3.9, the manual alignment of erroneous trials has allowed for the recognition of the distinctive shape of the ErrP. This result is consistent across all subjects, emphasizing a differentiated brain response between correct actions and actions where an error occurs. The data presented in the figure clearly indicate that the ErrP exhibits subject-specific variability in both amplitude and peak timing. This variability was expected, as each individual perceives and processes the generation of an error in unique ways and at different times.

However, from a visual standpoint, the trends of the displayed ErrPs indicate substantial similarity, highlighting the ability to generate this brain response under experimental conditions. The overall average across all subjects (see *Figure* 3.10) reveals a distinctive form of the ErrP. This differentiation between the two classes (erroneous and correct trials) is further underscored by the topoplots.

A comparison was made with the ErrP obtained in a similar experiment but with discrete control of the wheelchair. The results reveal a qualitative similarity in the waveform, as both display the two positive peaks separated by the negative peak. However, differences are evident in the amplitude of the positive peaks. It is hypothesized that the waveform similarity between the two control types can be attributed to the highly similar experimental protocol, suggesting an analogous brain response.

In a more in-depth comparison with studies on continuous control, a different waveform emerged. Specifically, considering Lopez's article [87], it is hypothesized that differences in the ErrP result from differently implemented experimental protocols. In the examined case, the ErrP was obtained by introducing an error in a continuous control context of a robotic arm. The main distinction lies in the fact that, during wheelchair control, unlike robotic arm control, the user is in direct contact with the controlled device and thus more engaged. The achieved results support the hypothesis that the form of the ErrP strictly depends on the type of task performed at the time of its generation.

Chapter 5

Conclusion

The study aimed to identify and describe the ErrPs during continuous control of a powered wheelchair. It can be stated that this objective was satisfactorily achieved: ErrP in this experimental context is present and well-defined, a result not yet documented in scientific literature. The characteristics of the ErrP align with signals generated during discrete control, with minimal differences in the occurrence of the positive peaks.

Inter-subject variability, arising from user driving style and attention during the experiment, posed an additional challenge for delay calculation. In future studies, an automatic method for delay calculation will need development, focusing on quantifying highly subjective and variable parameters constituting this measure.

The study involved only 9 subjects, making it statistically less robust. Future studies with the same objectives should include a larger number of participants. A positive aspect is the absence of restrictions in conducting the experiment, allowing the participation of subjects with diverse characteristics. It will be necessary to involve individuals with movement limitations to gather feedback on the experimental protocol and assess potential differences in brain response.

The development of a classifier will be essential to automatically identify the presence of ErrP. Implementing online classification would offer the advantage of immediately recording and correcting errors, altering the wheelchair's trajectory without incurring dangers.

In conclusion, the successful identification of ErrPs during the active control of a powered wheelchair opens new perspectives for advancing brain-machine interfaces. Despite analytical challenges and inter-subject variability, our study provides a solid foundation for future developments.

Bibliography

[1] M. M. Moore, "Real-world applications for brain-computer interface technology," *IEEE Transactions on Neural Systems and Rehabilitation Engineering*, vol. 11, no. 2, pp. 162–165, 2003.

[2] M. Arvaneh, C. Guan, K. K. Ang, *et al.*, "Facilitating motor imagery-based brain–computer interface for stroke patients using passive movement," *Neural Computing and Applications*, vol. 28, pp. 3259–3272, 2017.

[3] F Ortiz-Corredor, J. Silvestre-Avendano, and A Izquierdo-Bello, "Locked-in state mimicking cerebral death in a child with guillain-barre syndrome," *Revista de neurologia*, vol. 44, no. 10, pp. 636–638, 2007.

[4] I. K. Keme-Ebi and A. A. Asindi, "Locked–in syndrome in a nigerian male with multiple sclerosis: A case report and literature review," *Pan African Medical Journal*, vol. 1, no. 1, 2008.

[5] S. Moghimi, A. Kushki, A. Marie Guerguerian, and T. Chau, "A review of eeg-based brain-computer interfaces as access pathways for individuals with severe disabilities," *Assistive Technology*, vol. 25, no. 2, pp. 99–110, 2013.

[6] J. R. Wolpaw, D. J. McFarland, and T. M. Vaughan, "Brain-computer interface research at the wadsworth center," *IEEE transactions on rehabilitation engineering*, vol. 8, no. 2, pp. 222–226, 2000.

[7] F. H. Martini, M. J. Timmons, R. B. Tallitsch, *et al.*, *Anatomia umana / Frederic H. Martini, Michael J. Timmons, Robert B. Tallitsch; con William C. Ober ... [et al.] ; edizione italiana a cura di Lucio Cocco, Lucia Manzoli, Giovanni Zummo*, ita, 2. ed. Napoli: EdiSES, c2003, isbn: 88-7959-268-8.

[8] K. S. Saladin, S. Galli, R. De$_{C}aro$, K. S. Saladin, S. Galli, and R. De$_{C}aro$, *Anatomia umana / Kenneth S. Saladin*, ita, 2. ed. italiana sulla 5. americana / a cura di Raffaele De Caro ; con la collaborazione di Sergio Galli ... [et al.] Padova: Piccin, 2017, isbn: 9788829928323.

[9] R. D. Caro, A. Emmi, V. Macchi, *et al.*, *Lectures on Neuroanatomy: a Clinical and Morpho-Functional approach*, eng. CLEUP, 2021.

[10] L. Luo and L. Luo, *Principles of neurobiology / Liqun Luo*, eng. New York: Garland Science, 2016, isbn: 9780815344940.

[11] D. T. Stuss, "Traumatic brain injury: Relation to executive dysfunction and the frontal lobes," *Current opinion in neurology*, vol. 24, no. 6, pp. 584–589, 2011.

[12] K. Neulinger, J. Oram, H. Tinson, J. O'Gorman, and D. H. Shum, "Prospective memory and frontal lobe function," *Aging, Neuropsychology, and Cognition*, vol. 23, no. 2, pp. 171–183, 2016.

[13] M. Gabriel, L. Burhans, A. Talk, and P. Scalf, "Cingulate cortex," in *Encyclopedia of the Human Brain*, V. Ramachandran, Ed., New York: Academic Press, 2002, pp. 775–791, isbn: 978-0-12-227210-3. doi: https://doi.org/10.1016/B0-12-227210-2/00096-0. [Online]. Available: https://www.sciencedirect.com/science/article/pii/B0122272102000960.

[14] B. Hayden and M. Platt, "Cingulate cortex," in *Encyclopedia of Neuroscience*, L. R. Squire, Ed., Oxford: Academic Press, 2009, pp. 887–892, isbn: 978-0-08-045046-9. doi: https://doi.org/10.1016/B978-008045046-9.01110-4. [Online]. Available: https://www.sciencedirect.com/science/article/pii/B9780080450469011104.

[15] J. O'Neill, J. C. Piacentini, and B. S. Peterson, "Chapter 11 - cingulate role in tourette syndrome," in *Cingulate Cortex*, ser. Handbook of Clinical Neurology, B. A. Vogt, Ed., vol. 166, Elsevier, 2019, pp. 165–221. doi: https://doi.org/10.1016/B978-0-444-64196-0.00011-X. [Online]. Available: https://www.sciencedirect.com/science/article/pii/B978044464196000011X.

[16] K. R. Ridderinkhof, M. Ullsperger, E. A. Crone, and S. Nieuwenhuis, "The role of the medial frontal cortex in cognitive control," *science*, vol. 306, no. 5695, pp. 443–447, 2004.

[17] C. Im and J.-M. Seo, "A review of electrodes for the electrical brain signal recording," *Biomedical Engineering Letters*, vol. 6, pp. 104–112, 2016.

[18] F. Scholkmann, S. Kleiser, A. J. Metz, *et al.*, "A review on continuous wave functional near-infrared spectroscopy and imaging instrumentation and methodology," *Neuroimage*, vol. 85, pp. 6–27, 2014.

[19] G. Buzsáki, C. A. Anastassiou, and C. Koch, "The origin of extracellular fields and currents—eeg, ecog, lfp and spikes," *Nature reviews neuroscience*, vol. 13, no. 6, pp. 407–420, 2012.

[20] T. Ball, M. Kern, I. Mutschler, A. Aertsen, and A. Schulze-Bonhage, "Signal quality of simultaneously recorded invasive and non-invasive eeg," *Neuroimage*, vol. 46, no. 3, pp. 708–716, 2009.

[21] S. P. Levine, J. E. Huggins, S. L. BeMent, *et al.*, "Identification of electrocorticogram patterns as the basis for a direct brain interface," *Journal of clinical neurophysiology*, vol. 16, no. 5, p. 439, 1999.

[22] T. Yang, S. Hakimian, and T. H. Schwartz, "Intraoperative electrocorticography (ecog): Indications, techniques, and utility in epilepsy surgery," *Epileptic Disorders*, vol. 16, no. 3, pp. 271–279, 2014.

[23] E. Formaggio, S. F. Storti, V. Tramontano, *et al.*, "Frequency and time-frequency analysis of intraoperative ecog during awake brain stimulation," *Frontiers in Neuroengineering*, vol. 6, p. 1, 2013.

[24] R. S. Fisher and A. L. Velasco, "Electrical brain stimulation for epilepsy," *Nature Reviews Neurology*, vol. 10, no. 5, pp. 261–270, 2014.

[25] S. Baillet, J. C. Mosher, and R. M. Leahy, "Electromagnetic brain mapping," *IEEE Signal processing magazine*, vol. 18, no. 6, pp. 14–30, 2001.

[26] S. Debener, M. Ullsperger, M. Siegel, and A. K. Engel, "Single-trial eeg–fmri reveals the dynamics of cognitive function," *Trends in cognitive sciences*, vol. 10, no. 12, pp. 558–563, 2006.

[27] C. J. Aine, "A conceptual overview and critique of functional neuroimaging techniques in humans: I. mri/fmri and pet.," *Critical reviews in neurobiology*, vol. 9, no. 2-3, pp. 229–309, 1995.

[28] R. Elul, "The genesis of the eeg," *International review of neurobiology*, vol. 15, pp. 227–272, 1972.

[29] T. Kirschstein and R. Köhling, "What is the source of the eeg?" *Clinical EEG and neuroscience*, vol. 40, no. 3, pp. 146–149, 2009.

[30] W. M. Leach, "Fundamentals of low-noise analog circuit design," *Proceedings of the IEEE*, vol. 82, no. 10, pp. 1515–1538, 1994.

[31] G. L. Holmes and R. Khazipov, "Basic neurophysiology and the cortical basis of eeg," *The clinical neurophysiology primer*, pp. 19–33, 2007.

[32] A. L. Hodgkin and A. F. Huxley, "A quantitative description of membrane current and its application to conduction and excitation in nerve," *The Journal of physiology*, vol. 117, no. 4, p. 500, 1952.

[33] R. P. Balandong, R. F. Ahmad, M. N. M. Saad, and A. S. Malik, "A review on eeg-based automatic sleepiness detection systems for driver," *Ieee Access*, vol. 6, pp. 22 908–22 919, 2018.

[34] N Salansky, A Fedotchev, and A Bondar, "Responses of the nervous system to low frequency stimulation and eeg rhythms: Clinical implications," *Neuroscience & Biobehavioral Reviews*, vol. 22, no. 3, pp. 395–409, 1998.

[35] K. Zhang, W. Shi, C. Wang, *et al.*, "Reliability of eeg microstate analysis at different electrode densities during propofol-induced transitions of brain states," *NeuroImage*, vol. 231, p. 117 861, 2021.

[36] J. A. Pineda, "The functional significance of mu rhythms: Translating "seeing" and "hearing" into "doing"," *Brain research reviews*, vol. 50, no. 1, pp. 57–68, 2005.

[37] G. Pfurtscheller and C. Neuper, "Motor imagery and direct brain-computer communication," *Proceedings of the IEEE*, vol. 89, no. 7, pp. 1123–1134, 2001.

[38] X. Jia and A. Kohn, "Gamma rhythms in the brain," *PLoS biology*, vol. 9, no. 4, e1001045, 2011.

[39] S. Abenna, M. Nahid, and A. Bajit, "Motor imagery based brain-computer interface: Improving the eeg classification using delta rhythm and lightgbm algorithm," *Biomedical Signal Processing and Control*, vol. 71, p. 103 102, 2022.

[40] A. Kübler, B. Kotchoubey, J. Kaiser, J. R. Wolpaw, and N. Birbaumer, "Brain–computer communication: Unlocking the locked in.," *Psychological bulletin*, vol. 127, no. 3, p. 358, 2001.

[41] T. B. Sloan, L. Jameson, and D. Janik, "Chapter 7 - evoked potentials," in *Cottrell and Young's Neuroanesthesia (Fifth Edition)*, J. E. Cottrell and W. L. Young, Eds., Fifth Edition, Philadelphia: Mosby, 2010, pp. 115–130, isbn: 978-0-323-05908-4. doi: https://doi.org/10.1016/B978-0-323-05908-4.10012-0. [Online]. Available: https://www.sciencedirect.com/science/article/pii/B9780323059084100120.

[42] L. Sörnmo and P. Laguna, "Chapter 4 - evoked potentials," in *Bioelectrical Signal Processing in Cardiac and Neurological Applications*, ser. Biomedical Engineering, L. Sörnmo and P. Laguna, Eds., Burlington: Academic Press, 2005, pp. 181–336, isbn: 978-0-12-437552-9. doi: https://doi.org/10.1016/B978-012437552-9/50004-0.

[Online]. Available: https://www.sciencedirect.com/science/article/pii/B9780124375529500040.

[43] B. M. Abrams and H. J. Waldman, "14 - electromyography and evoked potentials," in *Practical Management of Pain (Fifth Edition)*, H. T. Benzon, J. P. Rathmell, C. L. Wu, D. C. Turk, C. E. Argoff, and R. W. Hurley, Eds., Fifth Edition, Philadelphia: Mosby, 2014, 162–184.e4, isbn: 978-0-323-08340-9. doi: https://doi.org/10.1016/B978-0-323-08340-9.00014-1. [Online]. Available: https://www.sciencedirect.com/science/article/pii/B9780323083409000141.

[44] D. Regan, "Human brain electrophysiology," *Evoked potentials and evoked magnetic fields in science and medicine*, 1989.

[45] A. Legatt, "Evoked potentials," in *Encyclopedia of the Neurological Sciences (Second Edition)*, M. J. Aminoff and R. B. Daroff, Eds., Second Edition, Oxford: Academic Press, 2014, pp. 228–231, isbn: 978-0-12-385158-1. doi: https://doi.org/10.1016/B978-0-12-385157-4.00529-7. [Online]. Available: https://www.sciencedirect.com/science/article/pii/B9780123851574005297.

[46] V. De Pascalis, "Chapter 16 - on the psychophysiology of extraversion," in *On the Psychobiology of Personality*, R. M. Stelmack, Ed., Oxford: Elsevier, 2004, pp. 295–327, isbn: 978-0-08-044209-9. doi: https://doi.org/10.1016/B978-008044209-9/50017-8. [Online]. Available: https://www.sciencedirect.com/science/article/pii/B9780080442099500178.

[47] J. D. Kropotov, A. Mueller, and V. A. Ponomarev, "Chapter 3 - erp-based endophenotypes: Application in diagnosis and neurotherapy," in *Neurofeedback and Neuromodulation Techniques and Applications*, R. Coben and J. R. Evans, Eds., San Diego: Academic Press, 2011, pp. 47–77, isbn: 978-0-12-382235-2. doi: https://doi.org/10.1016/B978-0-12-382235-2.00003-2. [Online]. Available: https://www.sciencedirect.com/science/article/pii/B9780123822352000032.

[48] S. Hillyard, "Event-related potentials (erps) and cognitive processing," in *Encyclopedia of Neuroscience*, L. R. Squire, Ed., Oxford: Academic Press, 2009, pp. 13–18, isbn: 978-0-08-045046-9. doi: https://doi.org/10.1016/B978-008045046-9.00311-9. [Online]. Available: https://www.sciencedirect.com/science/article/pii/B9780080450469003119.

[49] L. A. Farwell and E. Donchin, "Talking off the top of your head: Toward a mental prosthesis utilizing event-related brain potentials," *Electroencephalography and clinical Neurophysiology*, vol. 70, no. 6, pp. 510–523, 1988.

[50] E. Donchin and D. B. Smith, "The contingent negative variation and the late positive wave of the average evoked potential," *Electroencephalography and clinical Neurophysiology*, vol. 29, no. 2, pp. 201–203, 1970.

[51] D. J. McFarland, A. T. Lefkowicz, and J. R. Wolpaw, "Design and operation of an eeg-based brain-computer interface with digital signal processing technology," *Behavior Research Methods, Instruments, & Computers*, vol. 29, no. 3, pp. 337–345, 1997.

[52] G. Pfurtscheller and F. L. Da Silva, "Event-related eeg/meg synchronization and desynchronization: Basic principles," *Clinical neurophysiology*, vol. 110, no. 11, pp. 1842–1857, 1999.

[53] G. Pfurtscheller, C. Neuper, D. Flotzinger, and M. Pregenzer, "Eeg-based discrimination between imagination of right and left hand movement," *Electroencephalography and clinical Neurophysiology*, vol. 103, no. 6, pp. 642–651, 1997.

[54] N. Birbaumer, T. Elbert, A. G. Canavan, and B. Rockstroh, "Slow potentials of the cerebral cortex and behavior.," *Physiological reviews*, vol. 70, no. 1, pp. 1–41, 1990.

[55] M. Falkenstein, J. Hoormann, S. Christ, and J. Hohnsbein, "Erp components on reaction errors and their functional significance: A tutorial," *Biological Psychology*, vol. 51, no. 2, pp. 87–107, 2000, issn: 0301-0511. doi: https://doi.org/10.1016/S0301-0511(99)00031-9. [Online]. Available: https://www.sciencedirect.com/science/article/pii/S0301051199000319.

[56] C. Orr and R. Hester, "Error-related anterior cingulate cortex activity and the prediction of conscious error awareness," *Frontiers in human neuroscience*, vol. 6, p. 177, 2012.

[57] M. G. Coles, M. K. Scheffers, and C. B. Holroyd, "Why is there an ern/ne on correct trials? response representations, stimulus-related components, and the theory of error-processing," *Biological psychology*, vol. 56, no. 3, pp. 173–189, 2001.

[58] B. Blankertz, G. Dornhege, C. Schafer, *et al.*, "Boosting bit rates and error detection for the classification of fast-paced motor commands based on single-trial eeg analysis," *IEEE Transactions on Neural Systems and Rehabilitation Engineering*, vol. 11, no. 2, pp. 127–131, 2003.

[59] C. B. Holroyd and M. G. Coles, "The neural basis of human error processing: Reinforcement learning, dopamine, and the error-related negativity.," *Psychological review*, vol. 109, no. 4, p. 679, 2002.

[60] H. T. van Schie, R. B. Mars, M. G. Coles, and H. Bekkering, "Modulation of activity in medial frontal and motor cortices during error observation," *Nature neuroscience*, vol. 7, no. 5, pp. 549–554, 2004.

[61] A. Buttfield, P. Ferrez, and J. Millan, "Towards a robust bci: Error potentials and online learning," *IEEE Transactions on Neural Systems and Rehabilitation Engineering*, vol. 14, no. 2, pp. 164–168, 2006. doi: 10.1109/TNSRE.2006.875555.

[62] S. A. Swamy Bellary and J. M. Conrad, "Classification of error related potentials using convolutional neural networks," in *2019 9th International Conference on Cloud Computing, Data Science Engineering (Confluence)*, 2019, pp. 245–249. doi: 10.1109/CONFLUENCE.2019.8776901.

[63] W. J. Gehring, Y. Liu, J. M. Orr, and J. Carp, "The error-related negativity (ern/ne)," *Oxford handbook of event-related potential components*, pp. 231–291, 2012.

[64] S. Nieuwenhuis, K. R. Ridderinkhof, J. Blom, G. P. Band, and A. Kok, "Error-related brain potentials are differentially related to awareness of response errors: Evidence from an antisaccade task," *Psychophysiology*, vol. 38, no. 5, pp. 752–760, 2001.

[65] M. Falkenstein, J. Hohnsbein, J. Hoormann, and L. Blanke, "Effects of crossmodal divided attention on late erp components. ii. error processing in choice reaction tasks," *Electroencephalography and clinical neurophysiology*, vol. 78, no. 6, pp. 447–455, 1991.

[66] F. Iwane, I. Iturrate, R. Chavarriaga, and J. del R Millán, "Invariability of eeg error-related potentials during continuous feedback protocols elicited by erroneous actions at predicted or unpredicted states," *Journal of Neural Engineering*, vol. 18, no. 4, p. 046 044, 2021.

[67] S. Perdikis, L. Tonin, S. Saeedi, C. Schneider, and J. d. R. Millán, "The cybathlon bci race: Successful longitudinal mutual learning with two tetraplegic users," *PLoS biology*, vol. 16, no. 5, e2003787, 2018.

[68] A. N. Belkacem, N. Jamil, S. Khalid, and F. Alnajjar, "On closed-loop brain stimulation systems for improving the quality of life of patients with neurological disorders," *Frontiers in Human Neuroscience*, vol. 17, p. 1 085 173, 2023.

[69] C. Neuper and G. Pfurtscheller, "Neurofeedback training for bci control," *Brain-Computer Interfaces: Revolutionizing Human-Computer Interaction*, pp. 65–78, 2010.

[70] H.-J. Hwang, K. Kwon, and C.-H. Im, "Neurofeedback-based motor imagery training for brain–computer interface (bci)," *Journal of neuroscience methods*, vol. 179, no. 1, pp. 150–156, 2009.

[71] A. E. Hramov, V. A. Maksimenko, and A. N. Pisarchik, "Physical principles of brain–computer interfaces and their applications for rehabilitation, robotics and control of human brain states," *Physics Reports*, vol. 918, pp. 1–133, 2021.

[72] M. A. Lebedev and M. A. Nicolelis, "Brain–machine interfaces: Past, present and future," *TRENDS in Neurosciences*, vol. 29, no. 9, pp. 536–546, 2006.

[73] E. Fernández, A. Alfaro, C. Soto-Sánchez, *et al.*, "Visual percepts evoked with an intracortical 96-channel microelectrode array inserted in human occipital cortex," *The Journal of clinical investigation*, vol. 131, no. 23, 2021.

[74] J. Rickert, S. C. de Oliveira, E. Vaadia, A. Aertsen, S. Rotter, and C. Mehring, "Encoding of movement direction in different frequency ranges of motor cortical local field potentials," *Journal of Neuroscience*, vol. 25, no. 39, pp. 8815–8824, 2005.

[75] P. Konrad and T. Shanks, "Implantable brain computer interface: Challenges to neurotechnology translation," *Neurobiology of disease*, vol. 38, no. 3, pp. 369–375, 2010.

[76] F. Cincotti, D. Mattia, F. Aloise, *et al.*, "Non-invasive brain–computer interface system: Towards its application as assistive technology," *Brain research bulletin*, vol. 75, no. 6, pp. 796–803, 2008.

[77] R. Abiri, S. Borhani, E. W. Sellers, Y. Jiang, and X. Zhao, "A comprehensive review of eeg-based brain–computer interface paradigms," *Journal of neural engineering*, vol. 16, no. 1, p. 011 001, 2019.

[78] B. Z. Allison and C. Neuper, "Could anyone use a bci?" *Brain-computer interfaces: Applying our minds to human-computer interaction*, pp. 35–54, 2010.

[79] N. Padfield, K. Camilleri, T. Camilleri, S. Fabri, and M. Bugeja, "A comprehensive review of endogenous eeg-based bcis for dynamic device control," *Sensors*, vol. 22, no. 15, p. 5802, 2022.

[80] L. Yao, X. Sheng, D. Zhang, *et al.*, "A stimulus-independent hybrid bci based on motor imagery and somatosensory attentional orientation," *IEEE Transactions on Neural Systems and Rehabilitation Engineering*, vol. 25, no. 9, pp. 1674–1682, 2017.

[81] M. Alimardani, S. Nishio, and H. Ishiguro, "Brain-computer interface and motor imagery training: The role of visual feedback and embodiment," *Evolving BCI Therapy-Engaging Brain State. Dynamics*, vol. 2, no. 64, 2018.

[82] S. K. Mudgal, S. K. Sharma, J. Chaturvedi, and A. Sharma, "Brain computer interface advancement in neurosciences: Applications and issues," *Interdisciplinary Neurosurgery*, vol. 20, p. 100 694, 2020.

[83] C.-H. Han, Y.-W. Kim, D. Y. Kim, S. H. Kim, Z. Nenadic, and C.-H. Im, "Electroencephalography-based endogenous brain–computer interface for online communication with a completely locked-in patient," *Journal of neuroengineering and rehabilitation*, vol. 16, pp. 1–13, 2019.

[84] F.-B. Vialatte, M. Maurice, J. Dauwels, and A. Cichocki, "Steady-state visually evoked potentials: Focus on essential paradigms and future perspectives," *Progress in neurobiology*, vol. 90, no. 4, pp. 418–438, 2010.

[85] I. Batzianoulis, F. Iwane, S. Wei, *et al.*, "Customizing skills for assistive robotic manipulators, an inverse reinforcement learning approach with error-related potentials," *Communications biology*, vol. 4, no. 1, p. 1406, 2021.

[86] P. W. Ferrez and J. d. R. Millán, "Error-related eeg potentials generated during simulated brain–computer interaction," *IEEE transactions on biomedical engineering*, vol. 55, no. 3, pp. 923–929, 2008.

[87] C. Lopes-Dias, A. I. Sburlea, and G. R. Müller-Putz, "Online asynchronous decoding of error-related potentials during the continuous control of a robot," *Scientific reports*, vol. 9, no. 1, p. 17 596, 2019.

[88] L. Tonin, S. Perdikis, T. D. Kuzu, *et al.*, "Learning to control a bmi-driven wheelchair for people with severe tetraplegia," *iScience*, vol. 25, no. 12, p. 105 418, 2022, issn: 2589-0042. doi: https://doi.org/10.1016/j.isci.2022.105418. [Online]. Available: https://www.sciencedirect.com/science/article/pii/S258900422201690X.

[89] H. H. Jasper, "Ten-twenty electrode system of the international federation," *Electroencephalogr Clin Neurophysiol*, vol. 10, pp. 371–375, 1958.

[90] L. Zhang, W. He, C. He, and P. Wang, "Improving mental task classification by adding high frequency band information," *Journal of medical systems*, vol. 34, pp. 51–60, 2010.

[91] A. Koubâa *et al.*, *Robot Operating System (ROS)*. Springer, 2017, vol. 1.

[92] L. Tonin, G. Beraldo, S. Tortora, and E. Menegatti, "Ros-neuro: An open-source platform for neurorobotics," *Frontiers in Neurorobotics*, vol. 16, 2022, issn: 1662-5218. doi: 10.3389/fnbot.2022.886050. [Online]. Available: https://www.frontiersin.org/articles/10.3389/fnbot.2022.886050.

[93] W. J. Gehring, B. Goss, M. G. Coles, D. E. Meyer, and E. Donchin, "A neural system for error detection and compensation," *Psychological science*, vol. 4, no. 6, pp. 385–390, 1993.

[94] D. J. McFarland, L. M. McCane, S. V. David, and J. R. Wolpaw, "Spatial filter selection for eeg-based communication," *Electroencephalography and clinical Neurophysiology*, vol. 103, no. 3, pp. 386–394, 1997.

[95] A. López, F. Ferrero, D. Yangüela, C. Álvarez, and O. Postolache, "Development of a computer writing system based on eog," *Sensors*, vol. 17, no. 7, p. 1505, 2017.

[96] S.-H. Hsu, L. Pion-Tonachini, J. Palmer, M. Miyakoshi, S. Makeig, and T.-P. Jung, "Modeling brain dynamic state changes with adaptive mixture independent component analysis," *NeuroImage*, vol. 183, pp. 47–61, 2018.

Appendix A

Appendix A

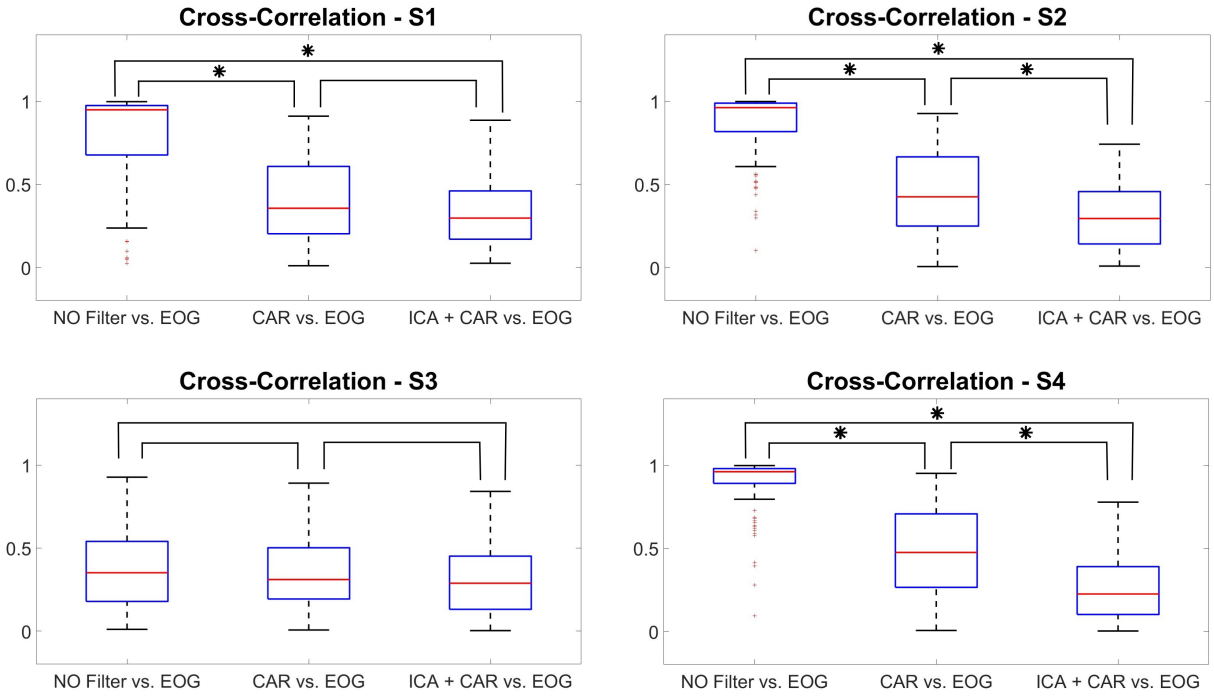

Figure A.1: *Cross-correlation indices for S1, S2, S3, and S4 related to all trials (Errors and Correct) of the EEG signal without CAR filter, with CAR filter and with CAR filter and AMICA vs. EOG signal. The asterisk means that the two corresponding correlation values are statistically different*

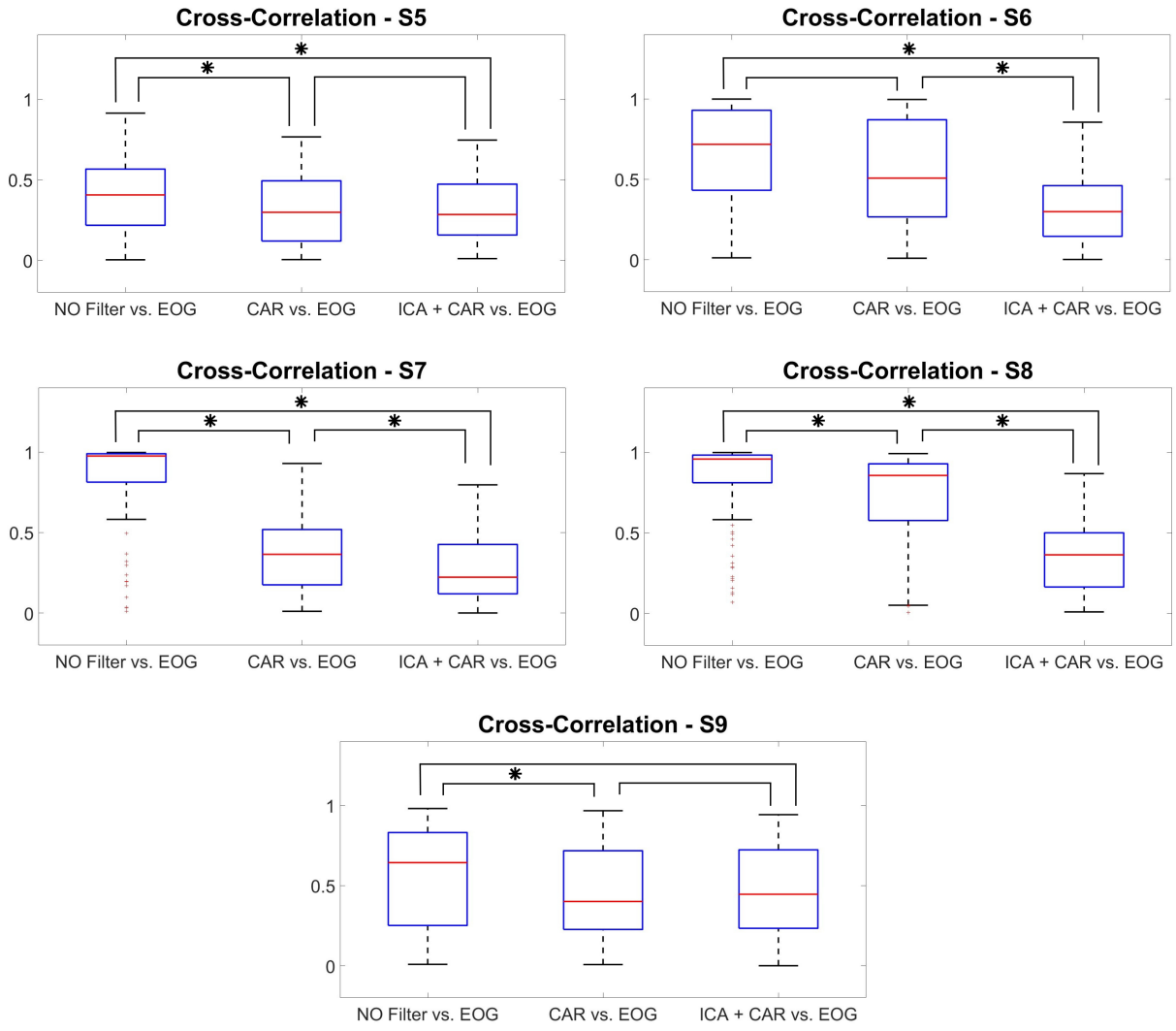

Figure A.2: *Cross-correlation indices for S1, S2, S3, S4, and S5 related to all trials (Errors and Correct) of the EEG signal without CAR filter, with CAR filter and with CAR filter and AMICA vs. EOG signal. The asterisk means that the two corresponding correlation values are statistically different*

Appendix B

Appendix B

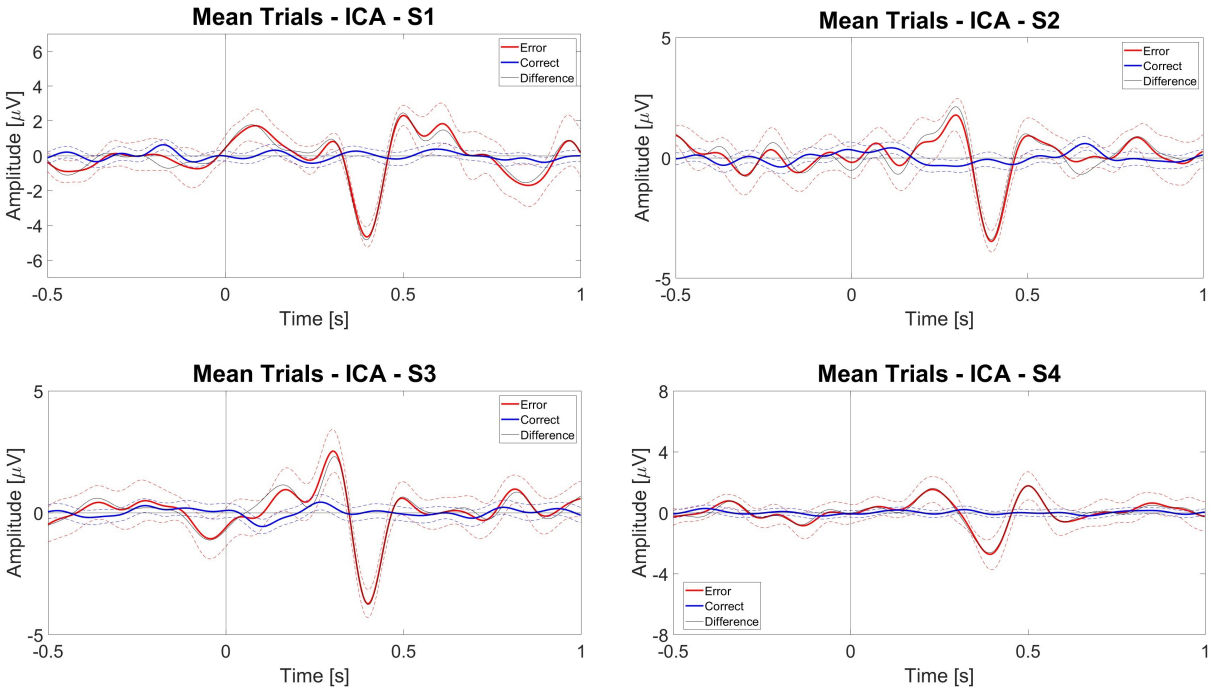

Figure B.1: *Average with standard deviation of Correct and Error Trials (blue and red lines, respectively) at channel FCz for S1, S2, S3, and S4. The signals were previously translated to manually align the negative peak of the Error Trials at 0.4 seconds.*

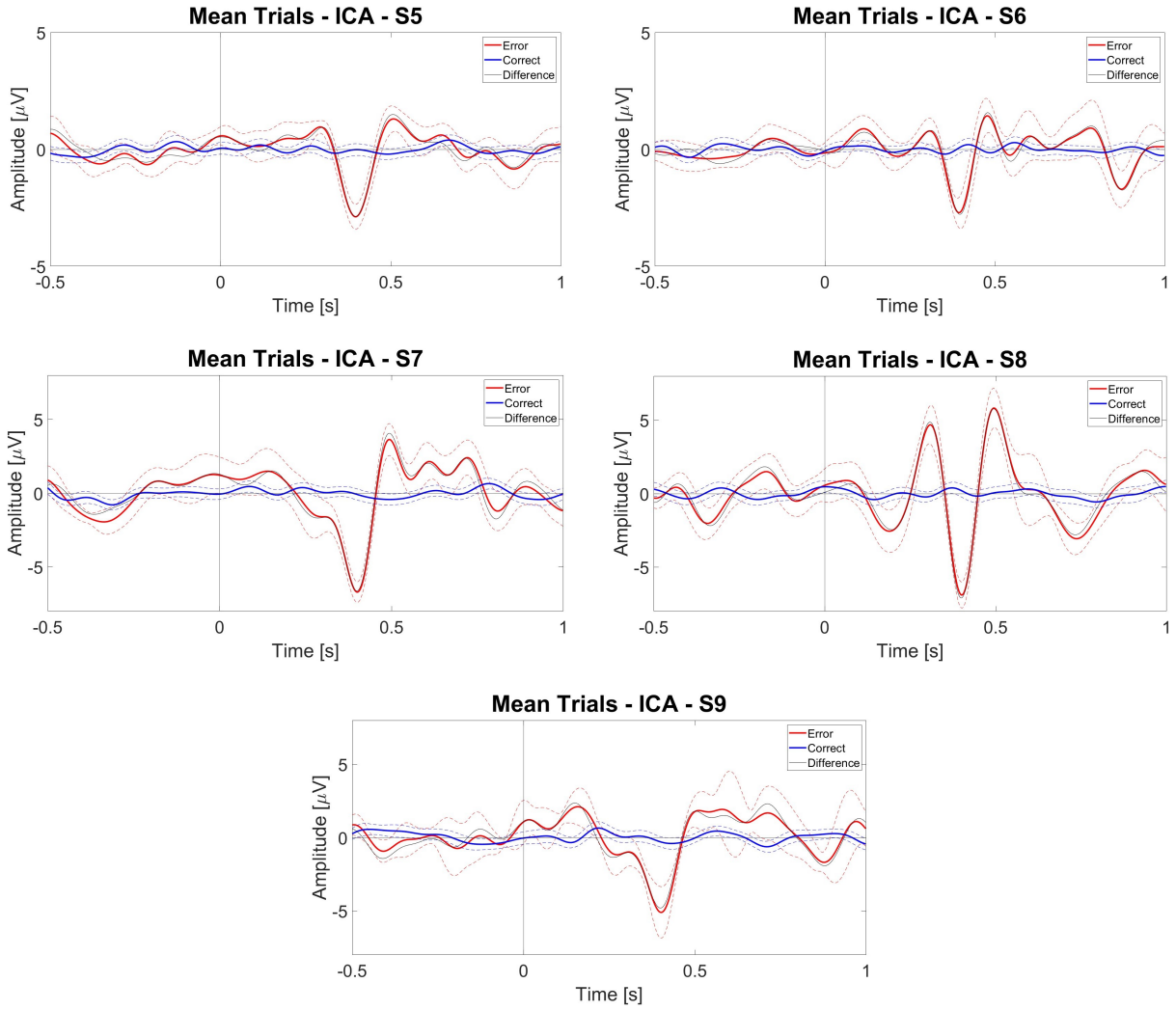

Figure B.2: *Average with standard deviation of Correct and Error Trials (blue and red lines, respectively) at channel FCz for S5, S6, S7, S8, and S9. The signals were previously translated to manually align the negative peak of the Error Trials at 0.4 seconds.*